Journal of Antimicrobial Chemotherapy

Antibiotic-induced degradation of antitoxin enhances the transcription of acetyltransferase-type toxin-antitoxin operon

Peifei Li[1], Ying-Xian Goh [1], Bojana Ilic[2], Cui Tai[1], Zixin Deng[1], Zhaoyan Chen[3], Marko Djordjevic[4] and Hong-Yu Ou [1]*

[1]State Key Laboratory of Microbial Metabolism, Joint International Laboratory on Metabolic & Developmental Sciences, School of Life Sciences & Biotechnology, Shanghai Jiao Tong University, Shanghai 200240, China; [2]Institute of Physics Belgrade, University of Belgrade, Belgrade 11000, Serbia; [3]Intensive Care Unit, First Affiliated Hospital of Guangxi Medical University, Nanning, Guangxi Province, 530021, China; [4]Quantitative Biology Group, Institute of Physiology and Biochemistry, Faculty of Biology, University of Belgrade, Belgrade 11000, Serbia

*Corresponding author. E-mail: hyou@sjtu.edu.cn

Background: Bacterial toxin-antitoxin (TA) modules respond to various stressful conditions. The Gcn5-related *N*-acetyltransferase-type toxin (GNAT) protein encoded by the GNAT-RHH TA locus is involved in the antibiotic tolerance of *Klebsiella pneumoniae*.

Objectives: To investigate the transcriptional mechanism of the GNAT-RHH operon *kacAT* under antibiotic stress.

Methods: The transcriptional level of the *kacAT* operon of *K. pneumoniae* was measured by quantitative real-time (qRT) PCR assay. The degradation of antitoxin KacA was examined by western blot and fluorescent protein. The ratio of [KacA]:[KacT] was calculated by the fluorescence intensity of KacA-eGFP and mCherry-KacT. Mathematical modelling predicted protein and transcript synthesis dynamics.

Results: A meropenem-induced increase in transcript levels of *kacA* and *kacT* resulted from the relief from transcriptional autoregulation of the *kacAT* operon. Meropenem induces the degradation of KacA through Lon protease, resulting in a reduction in the ratio of [KacA]:[KacT]. The decreased ratio causes the dissociation of the KacAT complex from its promoter region, which eliminates the repression of *kacAT* transcription. In addition, our dynamic model of *kacAT* expression regulation quantitatively reproduced the experimentally observed reduction of the [KacA]:[KacT] ratio and a large increase in *kacAT* transcript levels under the condition of strong promoter autorepression by the KacAT complex.

Conclusions: Meropenem promotes the degradation of antitoxin by enhancing the expression of Lon protease. Degradation of antitoxin reduces the ratio of intracellular [antitoxin]:[toxin], leading to detachment of the TA complex from its promoter, and releasing repression of TA operon transcription. These results may provide an important insight into the transcriptional mechanism of GNAT-RHH TA modules under antibiotic stress.

Introduction

After the discovery of the toxin-antitoxin (TA) modules on bacterial plasmids,[1] these TA modules were also found on prokaryotic chromosomes.[2,3] Depending on the nature of the antitoxin and its interaction with the toxin, TA modules have been recently divided into eight types (types I–VIII).[4] A typical type II TA module consists of a stable toxin protein and a metabolically unstable antitoxin protein, forming a non-toxic TA complex.[5,6] Some toxins contain a Gcn5-related *N*-acetyltransferase (GNAT) domain that can inhibit protein translation by acetylating aminoacyl tRNAs, such as AtaT,[7] AtaT2[8] and ItaT[9] from *Escherichia coli*, TacT,

TacT2 and TacT3 from *Salmonella enterica*[10–12] and GmvT from *Shigella flexneri*.[13] Their cognate antitoxin proteins possess a ribbon-helix-helix (RHH) domain. Our previous study showed that KacAT is a typical GNAT-RHH TA module present in the *K. pneumoniae* clinical isolate HS11286, where KacT can halt *K. pneumoniae* growth and induce antibiotic tolerance.[14,15]

Because TA modules are usually transcriptionally up-regulated under stressful conditions, many studies have proposed them as stress-response elements.[16–18] The transcription of type II TA operons is usually autoregulated by the toxin-antitoxin complex.[4] In such TA modules, toxin-antitoxin complexes with different affinities for the operon region are formed due to different ratios of

antitoxin to the toxin, with antitoxin-saturated complexes showing a high affinity for their promoter.[19–21] When the ratio of antitoxin to the toxin becomes smaller, the repression of TA complexes on their promoter is alleviated, the autoregulation of TA operons is relieved and the translation of TA modules is increased.[16,19–21] We have previously confirmed that antibiotics can increase the transcription of *kacT*, and the transcriptional level of *kacAT* was automatically regulated by the KacA:KacT ratio.[15,21] However, the transcriptional mechanism and autoregulation of the *kacAT* operon under antibiotic conditions are still unclear.

The C-terminal domain or the entire antitoxin protein is often irregular and highly sensitive to cellular protease. ATP-dependent proteases have been identified as the most important intracellular proteolytic enzymes, including the Lon (La) and ClpP protease families.[17,22] Although proteases can degrade antitoxins, evidence also shows that once the antitoxin forms a stable complex with its cognate toxin, it will either not be degraded or degraded very slowly.[23,24] Recently, a study reported that the presence of toxin protein YoeB and MpsR enhances the stability of antitoxin YefM and MqsA under a heat-shock condition.[16] However, no study has yet explored whether KacA in the GNAT-RHH family can be degraded under the antibiotic condition, and whether the degradation of KacA is related to *kacAT* transcription.

In this study, we found that the increase in *kacAT* transcription induced by the carbapenem antibiotic meropenem resulted from the deregulation of *kacAT* operon autoregulation. Degradation of KacA under the meropenem condition by Lon protease reduced the ratio of KacA to KacT, which caused the dissociation of the KacAT complex from its promoter region. Eventually, the repression of *kacAT* transcription by the KacAT complex was relieved.

Materials and methods

Strains and plasmids

Details of all the strains and plasmids used in this study are provided in Table S1 (available as Supplementary data at *JAC* Online), and all the oligonucleotides used in this study are listed in Table S2.

Tolerance assay

The tolerance to meropenem was tested by the cfu/mL count after exposure to meropenem. Overnight cultures of *K. pneumoniae* strains containing different pBAD33 derivatives were diluted in fresh LB medium at a ratio of 1:100. Cells were incubated at 37°C for 1 h, and 0.2% arabinose was added to the cultures to induce the expression of the *araBAD* promoter. After 90 min of incubation, meropenem was added to the cultures at 5 µg/mL. The cultures were incubated for another 4 h at the 37°C shaker. To determine cfu/mL, aliquots of 100 µL culture were serially diluted and spotted on the LB solid plates to calculate the surviving cells. The survival rate was calculated by dividing the cfu/mL in the culture after 4 h of incubation with the meropenem by the cfu/mL before adding the meropenem.[15,25,26]

Western blot

The cells treated with meropenem or serine hydroxamic acid (SHX) were collected and lysed by sonication in lysis buffer (25 mM Tris, 500 mM NaCl, 500 µM phenylmethylsulfonyl fluoride, pH 8.0). After centrifugation, the cleared supernatant was boiled with a loading buffer for 10 min. As for SDS-PAGE and immunoblotting, 60 µg protein was loaded per lane and separated by SDS-PAGE using 10% polyacrylamide gels. After

transferring the separated protein to the polyvinylidene fluoride membranes (PVDF; Merck Millipore, Germany), the PVDF membrane was blocked with 2.5% BSA in TBST (Tris-buffered saline with Tween-20: 30 mM Tris-base, 0.8% NaCl w/v, 0.1% Tween-20, pH 7.5) for 1 h at room temperature. Then, the PVDF membrane was washed three times with TBST and incubated with 6×His primary antibody at 4°C for a whole night. Following incubation, the PVDF membrane was washed three times using TBST and incubated with the corresponding second antibody at room temperature for 1 h. Finally, the PVDF membrane was washed with TBST and visualized by an automatic chemiluminescence image analysis system (Tanon 4600SF; Tanon, Shanghai, China).

LacZ activity assay

To construct the *lacZ* reporter plasmid, the *kacAT* promoter sequence was inserted upstream of the *lacZ* gene of a promoterless plasmid, pLACZ, forming the fusion plasmid pLACZ-P$_{kacAT}$. Different combinations of pLACZ-P$_{kacAT}$ and pBAD33 plasmid were co-transformed into RR2Δ(*kacAT lacZ*) and RR2Δ(*lon kacAT lacZ*) cells. The transformants were grown in an LB broth medium supplemented with 0.2% of arabinose for 3 h, then meropenem (5 µg/mL) and glucose (0.2%) were added. Samples for enzymatic activities were collected at the indicated time points (0, 15, 30 and 60 min). The β-galactosidase activity was measured according to the standard Miller method using chloroform and SDS to permeabilize the cells.[27]

### Quantitative real-time (q-RT)-PCR experiments

The total RNA of cells was extracted according to the manufacturer's instructions using the RNeasy Kit (Qiagen, Germany). After the digestion of genomic DNA using DNase I, 1000 ng RNA was converted to cDNA using PrimeScript™ RT Reagent Kit (Takara, Japan). qPCR reaction mix (BeyoFast™ SYBR Green qPCR Mix, Category No.: D7260-1 mL) was purchased from Beyotime Biotechnology (Shanghai, China), and the reactions were performed on an ABI 7500 instrument (Applied Biosystems). Each reaction was performed in triplicate simultaneously, and the fold change of gene expression was calculated using the $2^{-\Delta\Delta CT}$ method.[28] The housekeeping gene (glyceraldehyde-3-phosphate dehydrogenase, *KPHS_20800*) was used to normalize the expression levels of the different samples.

Results and discussion

Meropenem induces the transcription of kacA and kacT

We first explored the growth state of different *K. pneumoniae* strains under the meropenem condition. Figure S1a shows that, except for the wild-type *K. pneumoniae* HS11286 containing the carbapenemase gene (*bla*$_{KPC-2}$), the OD$_{600}$ of *bla*$_{KPC-2}$ gene deletion strain HS11286-RR2 and its derived strains was decreased gradually after 1 h of treatment, meaning that cells began to die and lyse. Thus, we treated the strains with meropenem for 0, 15, 30 and 60 min.

To see the effect of meropenem on *kacAT*'s transcription level, we examined the transcription of *kacA* and *kacT* in *K. pneumoniae* HS11286-RR2 (referred to as RR2 hereafter) under the exposure of meropenem (5 µg/mL). At the same time, as a chemical that can stimulate a stringent response in bacteria,[29] SHX (100 µg/mL) was used to represent stress other than antibiotic stress and was used as a comparison with meropenem. As shown in Figure 1, meropenem caused a significant increase in *kacT*'s transcriptional level, which is consistent with our previous study.[15] Meropenem also increased the transcriptional level of *kacA*
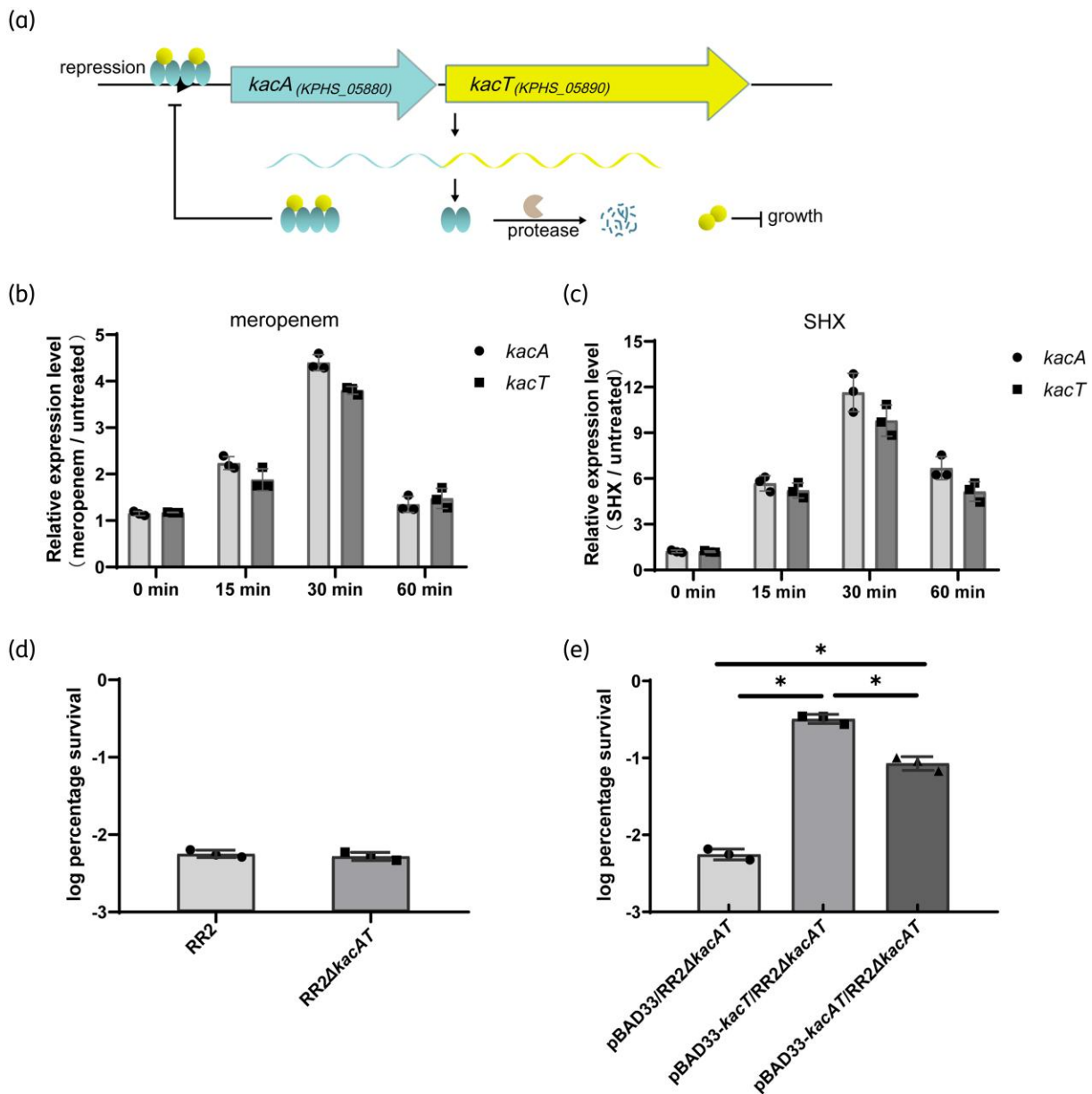
Figure 1. *kacAT* is involved in the response of *K. pneumoniae* to meropenem. (a) Schematic of acetyltransferase-type toxin-antitoxin pair, *kacAT*. *kacA* and *kacT* are co-transcribed. Two KacT molecules bind with four KacA molecules, forming a KacAT heterohexamer complex. The KacAT complex later binds and represses the *kacAT* promoter. KacT independently halts the growth of *K. pneumoniae*, whereas KacA can neutralize the toxicity of KacT. Proteases such as Lon can degrade KacA. Changes in *kacA* and *kacT* transcriptional levels responding to meropenem (b) or SHX (c) are depicted as measured by qRT-PCR. (d) The survival percentage of wild-type RR2 or *kacAT* knockout strain RR2*ΔkacAT*, treated by meropenem (5 μg/mL) for 4 h. (e) The survival percentage of RR2*ΔkacAT* strains harbouring empty vector pBAD33, KacT-expressing vector (pBAD33-*kacT*) or KacAT-expressing vector (pBAD33-*kacAT*) after exposure to 5 μg/mL meropenem for 4 h. The transcriptional levels of *kacA* and *kacT* genes were normalized using the house-keeping gene, *gapA*. The survival percentage was calculated by dividing the cfu/mL of the meropenem-treated culture by the cfu/mL of the culture before adding meropenem. SHX was used to compare with meropenem. The bar represents the mean of three independent experiments, and the error bar indicates the SD (*P value <0.05). This figure appears in colour in the online version of *JAC* and in black and white in the print version of *JAC*.

(Figure 1b). On the other hand, the transcriptional levels of *kacA* and *kacT* were also obviously enhanced by SHX (Figure 1c). These results indicated that, similar to other families of TA modules, the GNAT-RHH type TA module, KacAT, also responded to different stress conditions.

Overexpression of kacAT operon enhances the tolerance of K. pneumoniae to meropenem

The expression of the toxin gene *kacT* significantly inhibited the growth of *K. pneumoniae*, whereas the expression of *kacAT* or
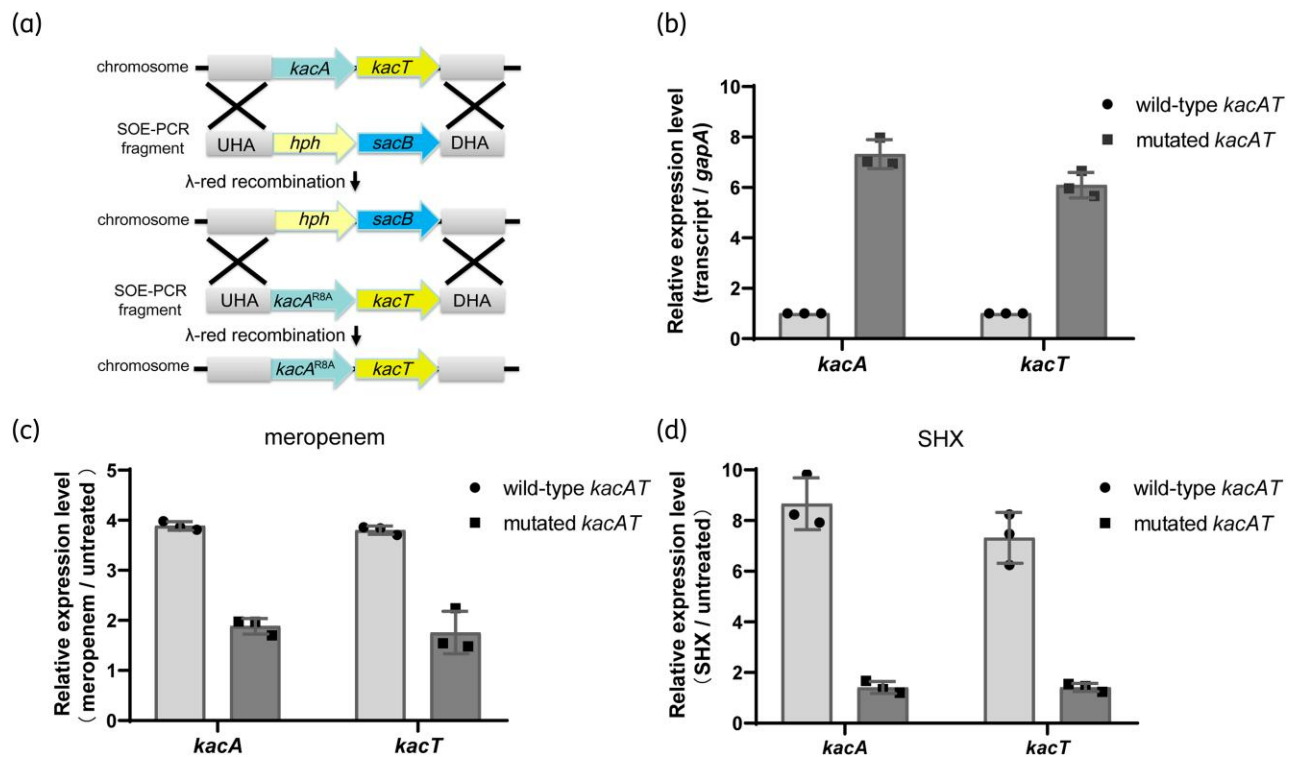
Figure 2. The increased transcription of *kacA* and *kacT* results from autoregulation relief under meropenem exposure. (a) Illustration of the method for constructing chromosomal point mutation strains. (b) Baseline transcriptional levels of *kacA* and *kacT* in wild-type RR2 and mutated KacA[R8A] strains under the normal condition. (c, d) Transcription levels of *kacA* and *kacT* in wild-type RR2 and mutated KacA[R8A] strains under stress conditions. SHX was used to compare with meropenem. Data are presented as mean ± SD (error bars); $n = 3$. DHA, downstream homologous arm; *hph*, hygromycin resistance gene; SOE, gene splicing by overlap extension; UHA, upstream homologous arm; λ-red, phage λ Red recombinase (gam, bet, exo). This figure appears in colour in the online version of *JAC* and in black and white in the print version of *JAC*.

empty pBAD33 plasmid did not (Figure S1b and c). Additionally, we previously found that KacT overexpression induced meropenem tolerance in *K. pneumoniae*.[15] However, the effect of the *kacAT* operon on meropenem tolerance remains to be elucidated. We examined whether the *kacAT* operon affects meropenem tolerance in RR2. As Figure 1d shows, the survivability of RR2 under meropenem exposure was not affected, disregarding the presence of the *kacAT* operon. It is worth noting that, except for KacT, overexpression of KacAT also induced meropenem tolerance in RR2Δ*kacAT* regardless of meropenem concentration (Figure 1e and Figure S1d). The enzymatic activity (detected by the WST-1 cell proliferation and cytotoxicity assay kit) of meropenem-treated *K. pneumoniae* HS11286-RR2Δ*kacAT* was significantly decreased, but the enzymatic activity of strains expressing KacT or KacAT was higher than that of the strain expressing the empty plasmid (Figure S1e). Additionally, we found that the overexpression of KacT and KacAT also increased the tolerance of RR2Δ*kacAT* to imipenem (Figure S1f).
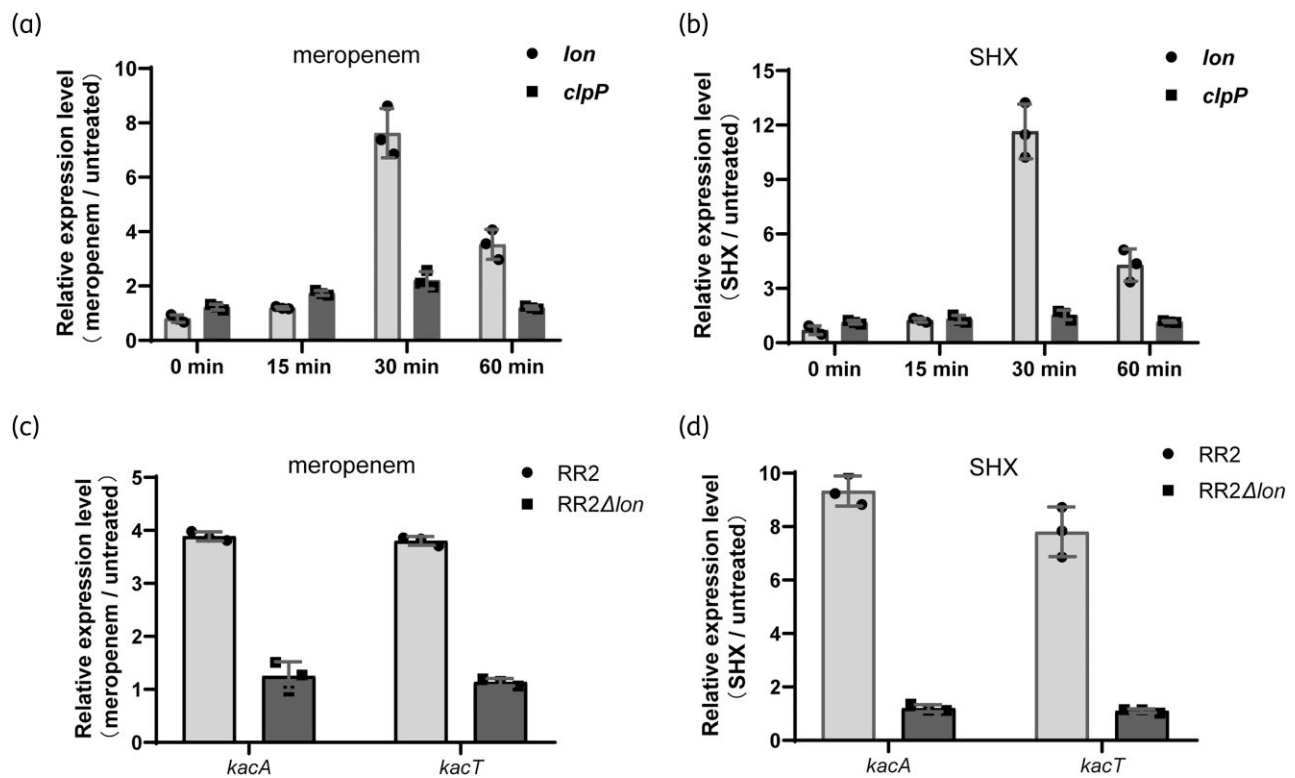
Meropenem-induced *kacAT* transcription results from relief from autoregulation

Type II TA modules strictly obey transcriptional autoregulation performed through conditional cooperativity.[5] We have previously reported that the transcriptional level of *kacAT* is autoregulated

by the [KacA]:[KacT] ratio.[21] Hence, we constructed a chromosomal point mutation in a KacA residue (KacA[R8A]). The residue is required for DNA binding, and the mutated KacA loses the ability to bind its promoter.[21] Then, we measured the transcriptional level of *kacA* and *kacT* under normal or stress conditions using the wild-type RR2 strain, and the KacA-mutated strain (KacA[R8A]). The baseline expression levels of *kacA* and *kacT* in mutated strains were elevated compared with that in the wild-type RR2 strain (Figure 2b). However, the mutated strain's *kacA* and *kacT* transcriptional levels no longer significantly increased, as with the wild-type strain (Figure 2c and d). These results indicated that, under the meropenem condition, relief of *kacAT* autoregulation can increase *kacA* and *kacT* transcription levels in the wild-type RR2 strain.

Lon protease affects transcription of the *kacAT* operon under the meropenem condition

It is proposed that proteases such as Lon or ClpP can degrade antitoxins, freeing toxins to regulate bacterial growth.[17] To test whether the protease genes (*lon* and *clpP*) in RR2 were up-regulated after meropenem treatment, the transcript levels of *lon* and *clpP* were quantified. As shown in Figure 3, the transcription of *lon* increased gradually after meropenem or SHX treatment whereas the transcription level of *clpP* remained constant

Figure 3. Meropenem induces *lon* transcription that eventually affects *kacAT* transcription. Changes in the *clpP* and *lon* transcription levels in response to meropenem (a) or SHX (b) were measured using qRT-PCR. The transcriptional levels of *kacA* and *kacT* in wild-type RR2 and *lon*-deleted RR2Δ*lon* strain under exposure to meropenem (c) or SHX (d) are depicted. Transcriptional levels of *lon*, *clpP*, *kacA* and *kacT* were normalized using the housekeeping gene *gapA*. SHX was used to compare with meropenem. Data are presented as mean ± SD (error bars); *n* = 3.

(Figure 3a and b). Using the wild-type RR2 and RR2Δ*lon* strains, we further examined the effect of *lon* on *kacAT's* transcription after meropenem exposure. Our results showed that the transcription levels of *kacA* and *kacT* in the RR2Δ*lon* strain were remarkably lower than in the wild-type RR2 strain after meropenem or SHX exposure (Figure 3c and d). These results suggest that *lon* is transcribed at a higher rate under meropenem exposure, possibly translating more Lon protease that could affect *kacA* and *kacT* transcription.
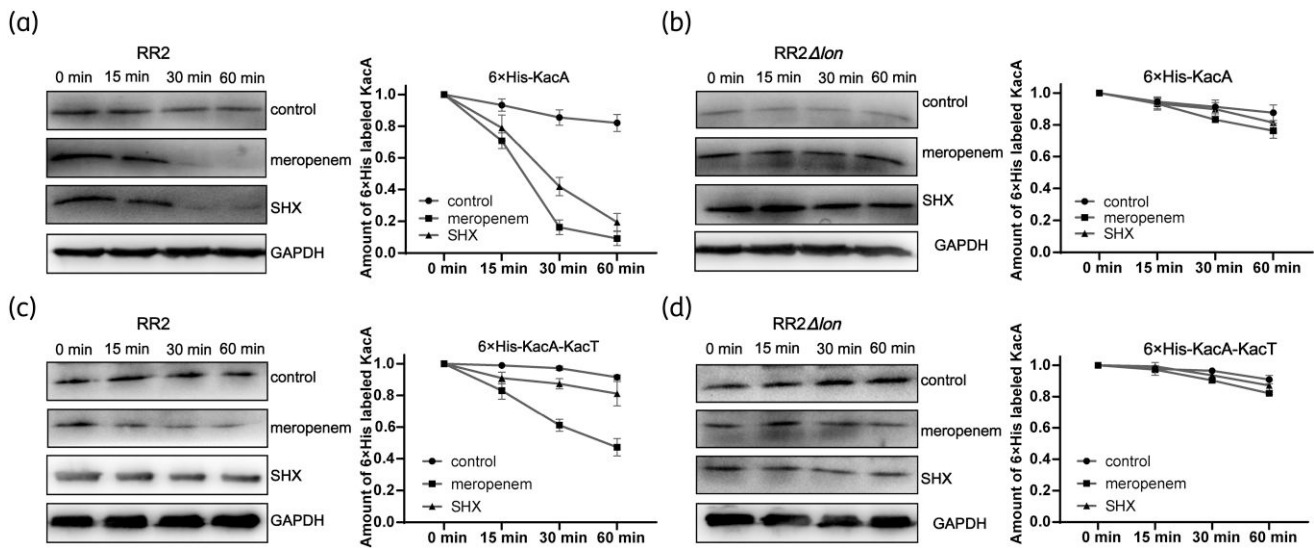
Meropenem leads to KacA degradation through Lon protease

The *in vivo* degradation rate of KacA was examined. We first used western blotting to explore the stability of KacA under meropenem conditions. In the wild-type RR2 cells, compared with the untreated control group, the 6×His-KacA was significantly degraded after meropenem or SHX treatment (Figure 4a). In contrast, for the RR2Δ*lon* cells, the 6×His-KacA did not degrade as much as in RR2 cells (Figure 4b).

Furthermore, it was reported that the existence of toxins YoeB and MqsR can improve the stability of their cognate antitoxins YefM and MqsA, respectively, under heat-shock conditions.[16] However, in another independent study, the authors demonstrated that the antitoxin HipB2 in *Caulobacter* was degraded, although the cognate toxin HipA2 was also present.[30] We thus

explored whether the existence of KacT can slow the degradation rate of KacA. We showed that, in the presence of KacT, KacA did not show visible degradation under SHX pressure, which is consistent with a previous report.[16] Nevertheless, significant degradation of KacA still occurred under the meropenem condition, although the degradation rate was slower than in the absence of KacT (Figure 4c). Apart from that, the 6×His-KacA in RR2Δ*lon* cells did not obviously degrade when KacT was present (Figure 4d). These results suggest that, under the meropenem condition, Lon protease can degrade KacA regardless of the presence of KacT.

We also used fluorescent protein to detect the stability of KacA. We first explored the influence of fluorescent protein on the normal function of KacA and KacT. From Figure S2a, we see that only KacT fused to mCherry at the N-terminal (mCherry-KacT) could inhibit the growth of *K. pneumoniae* similarly to wild-type KacT. KacA fused to eGFP at either N-terminal or C-terminal (eGFP-KacA and KacA-eGFP) could relieve the inhibition of *K. pneumoniae* growth by KacT (Figure S2b). We also found that both eGFP-KacA and KacA-eGFP could neutralize mCherry-KacT's toxicity (Figure S2c). Additionally, the complex formed by KacA-eGFP and mCherry-KacT could bind to P*kacAT* and inhibit the translation of LacZ (Figure S2d). We also observed the *in vivo* expression of KacA-eGFP and mCherry-KacT (Figure S3a). Furthermore, the stability of KacA-eGFP was measured by using a microplate reader. After treatment with

Figure 4. Meropenem induces KacA degradation through Lon protease. Wild-type RR2 and *lon*-deletion (RR2*Δlon*) strains harbouring the pBAD33 vector that expresses (a, b) only 6×His-KacA and (c, d) with KacT. The strains were grown in LB medium at 37°C, $OD_{600} = 0.3$, with 0.2% (w/v) of arabinose. After 90 min of induction, 0.2% (w/v) of glucose was added to inhibit KacA expression together with meropenem. Samples for western blot were collected at the indicated time points (0, 15, 30 and 60 min). (a) and (b) show that the free KacA is degraded by Lon protease after meropenem exposure. (c) and (d) show that KacT could not stabilize KacA under meropenem exposure. SHX was used to compare with meropenem. Data are presented as mean ± SD (error bars); $n = 3$. GAPDH, Glyceraldehyde-3-phosphate dehydrogenase.
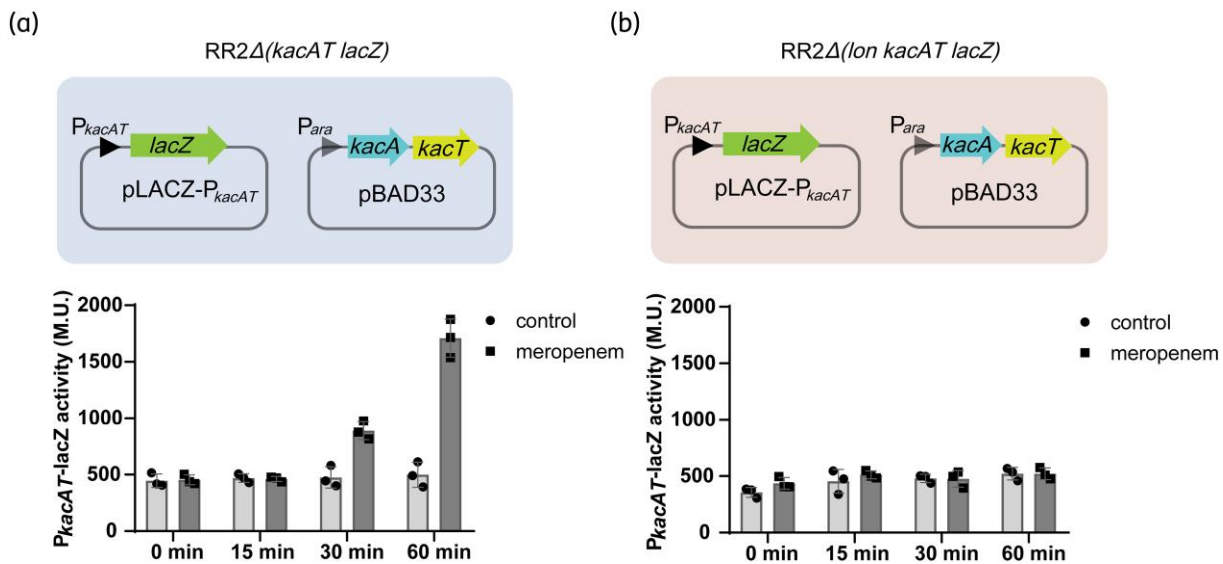
Figure 5. Meropenem promotes the dissociation of the KacAT complex from its promoter. *kacAT* promoter (P_{kacAT}) and the downstream *lacZ* were cloned on the pLACZ-P_{kacAT} plasmid, whereas *kacA* and *kacT* were on the pBAD33 plasmid. pLACZ-P_{kacAT} and pBAD33 in combination expressing KacA and KacT were co-transformed into RR2*Δ(kacAT lacZ)* (a) and RR2*Δ(lon kacAT lacZ)* (b) cells. Meropenem and 0.2% glucose were added after 3 h of induction of KacA and KacT by arabinose (0.2%). Samples for enzymatic activities were collected at the indicated timepoints (0, 15, 30 and 60 min). MU, miller unit. This figure appears in colour in the online version of *JAC* and in black and white in the print version of *JAC*.

meropenem or SHX, the fluorescence intensity of KacA-eGFP was significantly decreased in the wild-type RR2 compared with RR2*Δlon* cells (Figure S3b and c). Despite the presence of KacT, the fluorescence intensity of KacA-eGFP in wild-type RR2 was still significantly reduced after meropenem treatment compared with the RR2*Δlon* strain (Figure S3d and e), which is consistent with the results of western blot. Besides, we also found that imipenem caused reduced fluorescence intensity of KacA-eGFP in wild-type RR2 compared with RR2*Δlon* cells, which implies that imipenem can also induce the degradation of KacA (Figure S4).

(a)

(b)

(c)
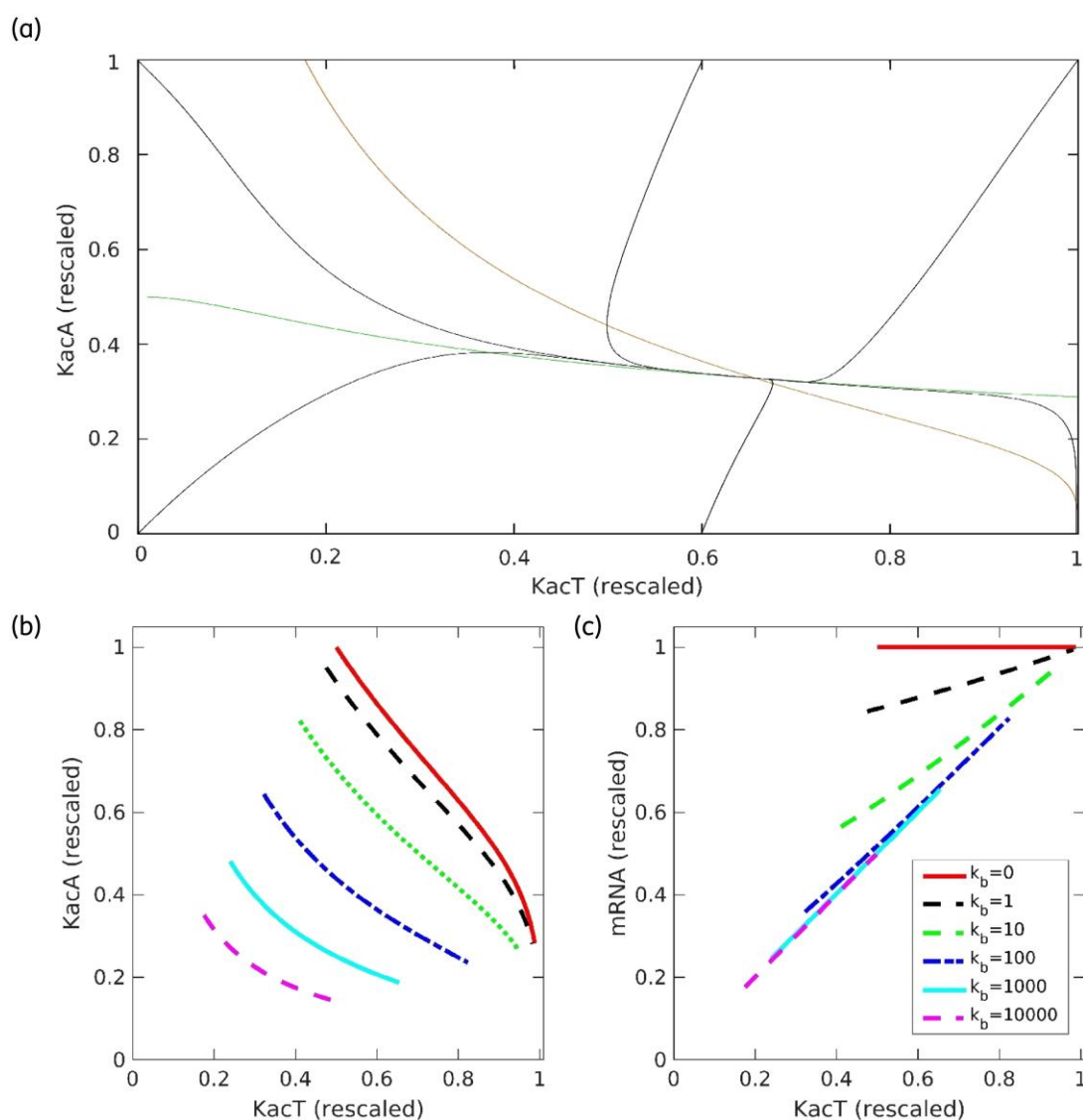
Figure 6. Result of modeling *kacAT* expression dynamics. Phase plane analysis of the system dynamics for the rescaled parameter values $\tilde{\varphi} = 1$, $\tilde{K}_T = 1$, $\tilde{K}_B = 100$, $\Delta\tilde{\lambda} = 3$ (see Materials and methods). The orange and green curves correspond to KacA and KacT nullclines, respectively, with their intersection determining the system's steady state. Solid black curves present trajectories for different system initial conditions (a). Equilibrium values of KacA versus KacT (b) and *kacAT* mRNA versus KacT (c). Different curves correspond to different $\tilde{K}_B$ values indicated in the legend. Points on each curve correspond to changing $\Delta\tilde{\lambda}$ from 0 (left edge) to 6 (right edge), and the values on the axes are rescaled. This figure appears in colour in the online version of *JAC* and in black and white in the print version of *JAC*.

Additionally, we studied whether meropenem could induce KacT's degradation. Under meropenem treatment, the non-toxic KacT[Y145F] in RR2 or RR2*Δlon* did not degrade much (Figure S5a and b). Likewise, the fluorescence intensity of mCherry-KacT[Y145F] in wild-type RR2 did not change after meropenem treatment (Figure S5c and d).

Meropenem promotes dissociation of the KacAT complex from its promoter

Because meropenem can promote the degradation of KacA but not KacT, meropenem likely alters the intracellular ratio of [KacA]:[KacT]. To our knowledge, the change in antitoxin to toxin ratio has not been successfully investigated *in vivo* although some approaches have been tried such as the pulse-chase assay.[16] We initially used western blotting to explore changes in the [KacA]:[KacT] ratio but also failed (data not shown). Hence, we fused KacA and KacT with eGFP and mCherry, respectively. The fluorescence intensity of KacA-eGFP and mCherry-KacT, under meropenem stress, was measured by a microplate reader. Our results showed that the ratio of remaining KacA-eGFP to mCherry-KacT was significantly reduced in the wild-type RR2 under the meropenem condition (Figure S6a). Meanwhile, the ratio of [KacA]:[KacT] in the *lon* deletion strain remained unchanged (Figure S6b).
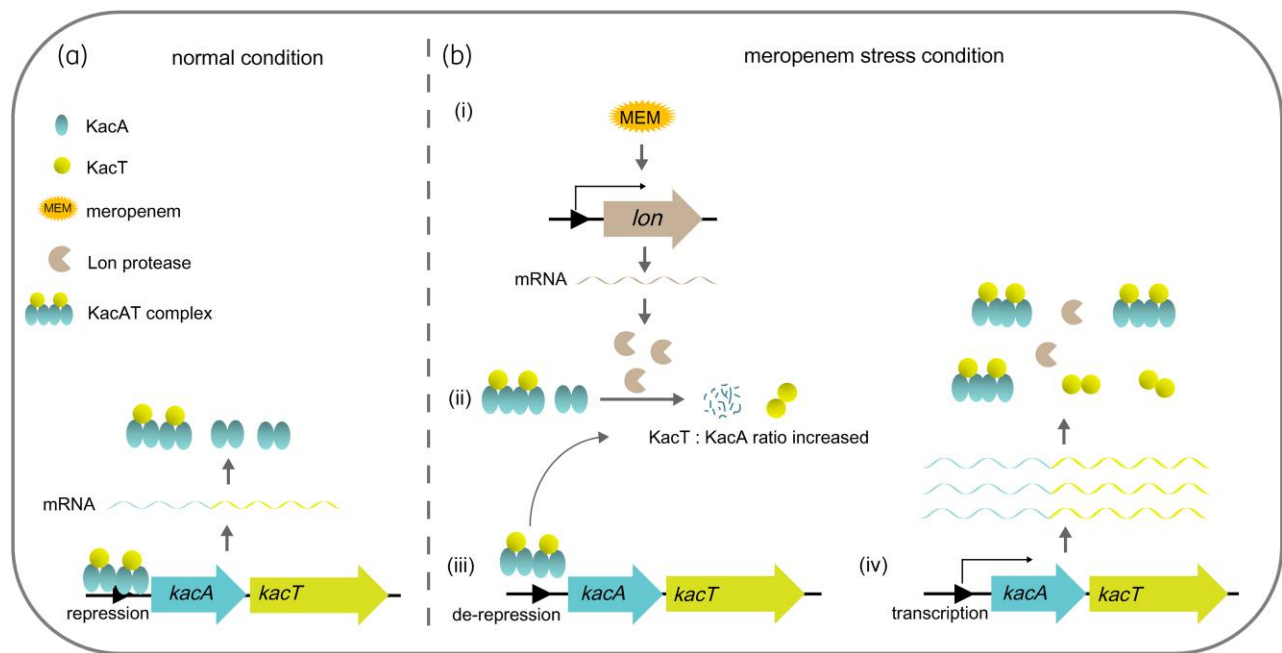
Figure 7. Transcription of the *kacAT* operon under the normal condition (a) and the meropenem stress (b). Meropenem (MEM) induces the enhanced expression of Lon protease, which degrades KacA, resulting in a reduction in the ratio of KacA:KacT. Then, the KacAT complex dissociates from its promoter region, and the transcription of *kacA* and *kacT* is elevated. This figure appears in colour in the online version of *JAC* and in black and white in the print version of *JAC*.

Due to the reduced ratio of [KacA]:[KacT] caused by meropenem, we suggest that meropenem can promote the dissociation of the KacAT complex from its promoter region. We performed a LacZ activity experiment in the *kacAT* promoter (P*kacAT*). Our results showed that, with the prolongation of meropenem treatment time, LacZ activity in RR2Δ(*kacAT lacZ*) harbouring KacA and KacT increased, whereas the RR2Δ(*lon kacAT lacZ*) did not (Figure 5). Additionally, in RR2Δ(*kacAT lacZ*) and RR2Δ(*lon kacAT lacZ*) containing the empty pBAD33 plasmid, LacZ activity was also unchanged under the meropenem conditions (Figure S7). A plausible explanation is that, under meropenem conditions, the KacAT complex dissociates from its promoter P*kacAT*, leading to the transcription of LacZ.

A quantitative model of kacAT expression dynamics explains experimental observations

Based on the experimental results presented above, we developed a quantitative model that can predict protein and transcript synthesis dynamics (see Supplemental methods). We aimed to achieve the following through the model: (1) Check if and under what conditions (parameter range) the model can explain the experimentally observed system response to antibiotic stress, in particular, the significant increase in *kacAT* transcript amounts and the decrease in [KacA]:[KacT] ratio. (2) Predict the dynamics of KacT under antibiotic stress, i.e. upon an increase in KacA degradation. In particular, we aimed to understand the somewhat perplexing observation that KacAT overexpression induces antibiotic stress tolerance, whereas *kacAT* deletion does not affect this tolerance. (3) Infer general properties of *kacAT* expression

dynamics, such as the steady state's number and stability, and how the steady states change with changing parameter values (which is also related to the two previous points).

We start with (3) above, with Figure 6a presenting the phase space analysis of the system dynamics. The system has one steady state corresponding to the intersection of the two nullclines (the orange and the green curves). Linear stability analysis leads to two negative real eigenvalues for this steady state, corresponding to a stable node. Figure 6a shows that trajectories with different initial conditions converge to this stable node. As the system parameters are changed, the phase space topology does not change, but the position of the steady state changes its location in the phase space (not shown in Figure 6a).

We next analyse how the steady state changes as $\Delta\tilde{\lambda}$ (scaled degradation rate of KacA) and $\tilde{K}_B$ (scaled binding affinity of KacAT complex to the promoter) are changed. $\Delta\tilde{\lambda}$ is variable as the experimental analysis found that, via this parameter, the antibiotic stress influences the system dynamics, where $\Delta\tilde{\lambda}$ is changed from 0 (the absence of antibiotic stress) to the relatively high value of $\Delta\tilde{\lambda} = 6$. It is also clear that $\tilde{K}_B$ is a crucial parameter controlling system behaviour, given the reported derepression of the promoter upon antibiotic stress. $\tilde{K}_B = 0$ corresponds to a constitutive (unregulated) promoter, allowing investigation of the system's behaviour during overexpression experiments. Similarly, high values of $\tilde{K}_B$ correspond to strong KacAT complex binding to the promoter, and we change $\tilde{K}_B$ on an exponential scale from 0 to 10^4 (see legend for Figure 6c).

Figure 6b and c show how (rescaled) equilibrium values of KacA, KacT and *kacAT* mRNA change with variations of $\Delta\tilde{\lambda}$ and $\tilde{K}_B$. For each curve, the left edge corresponds to $\Delta\tilde{\lambda} = 0$, and the

right edge to $\Delta\tilde{\lambda} = 6$, and different curves correspond to different $\tilde{K}_B$ values (see the legend). In Figure 6b, we see that irrespective of $\tilde{K}_B$, the ratio [KacA]:[KacT] decreases as $\Delta\tilde{\lambda}$ increases, consistent with experimental observations. Moreover, we obtain a robust (independent of parameter values) prediction that antibiotic stress leads to decreased KacA and increased KacT. This prediction is non-trivial because the decrease of the [KacA]:[KacT] ratio can also be realized through other scenarios, e.g. if KacT remains constant or even decreases, accompanied by a faster decline of KacA.

Figure 6c shows *kacAT* mRNA versus KacT steady-state values. Different lines correspond to different $\tilde{K}_B$ values, and points on each line correspond to increasing (from left to right along the lines) $\Delta\tilde{\lambda}$ values. The horizontal (topmost) line corresponds to the constitutive promoter ($\tilde{K}_B=0$), i.e. to the conditions of the overexpression experiment. The figure shows that smaller $\tilde{K}_B$ values do not lead to a significant increase in the transcript amounts, contrary to what was experimentally observed. Consequently, the strong binding of the complex to the promoter (high $\tilde{K}_B$ values) is consistent with the experimental results. Interestingly, for high $\tilde{K}_B$ values (see the bottommost line corresponding to $\tilde{K}_B = 10^4$), the highest value of KacT (the right edge of the line, obtained for the highest value of $\Delta\tilde{\lambda}$) is still smaller than the lowest KacT value (the left line edge corresponding to $\Delta\tilde{\lambda} = 0$) in the constitutive case. This prediction might explain the naively surprising result that the overexpression experiment led to antibiotic stress tolerance, which is not the case for the native (autoregulated) system. That is, due to the strong binding affinity of the repression complex to promoter DNA, even a significant increase in KacA degradation rate might not be enough to achieve large enough KacT levels necessary to observe antibiotic tolerance.

Transcriptional mechanism of the kacAT operon under meropenem stress

Based on the above, we propose a putative model that explains the transcriptional mechanism of the *kacAT* operon under the meropenem condition (Figure 7). In normal circumstances, the relatively lower translation efficiency of KacT ensures the amount of KacA molecules is more than that of KacT. KacA molecules counteract all KacT molecules to form the KacAT complex without releasing the toxicity of KacT. The KacAT complex can bind to its promoter DNA region and block the transcription of *kacAT*. Once the living conditions are changed, such as in meropenem stress, the transcriptional level of the Lon protease gene is increased, resulting in the degradation of unstable KacA. Due to the degradation of KacA, the ratio of [KacA]:[KacT] becomes <1, and the KacAT complex subsequently dissociates from the promotor region of the *kacAT* operon, thereby relieving repression of *kacAT* transcription.

Supplementary data

Figures S1 to S7, Tables S1 and S2, and Supplemental methods are available as Supplementary data at *JAC* Online.

References

1 Gerdes K, Rasmussen PB, Molin S. Unique type of plasmid maintenance function: postsegregational killing of plasmid-free cells. *Proc Natl Acad Sci U S A* 1986; **83**: 3116–20. https://doi.org/10.1073/pnas.83.10.3116

2 Xie Y, Wei Y, Shen Y *et al.* TADB 2.0: an updated database of bacterial type II toxin-antitoxin loci. *Nucleic Acids Res* 2018; **46**: D749–D53. https://doi.org/10.1093/nar/gkx1033

3 Shao Y, Harrison EM, Bi D *et al.* TADB: a web-based resource for type 2 toxin-antitoxin loci in bacteria and archaea. *Nucleic Acids Res* 2011; **39**: D606–D11. https://doi.org/10.1093/nar/gkq908

4 Jurenas D, Fraikin N, Goormaghtigh F *et al.* Biology and evolution of bacterial toxin-antitoxin systems. *Nat Rev Microbiol* 2022; **20**: 335–50. https://doi.org/10.1038/s41579-021-00661-1

5 Harms A, Brodersen DE, Mitarai N *et al.* Toxins, targets, and triggers: an overview of toxin-antitoxin biology. *Mol Cell* 2018; **70**: 768–84. https://doi.org/10.1016/j.molcel.2018.01.003

6 Page R, Peti W. Toxin-antitoxin systems in bacterial growth arrest and persistence. *Nat Chem Biol* 2016; **12**: 208–14. https://doi.org/10.1038/nchembio.2044

7 Jurenas D, Chatterjee S, Konijnenberg A *et al.* Atat blocks translation initiation by N-acetylation of the initiator tRNA^{fMet}. *Nat Chem Biol* 2017; **13**: 640–6. https://doi.org/10.1038/nchembio.2346

8 Ovchinnikov SV, Bikmetov D, Livenskyi A *et al.* Mechanism of translation inhibition by type II GNAT toxin AtaT2. *Nucleic Acids Res* 2020; **48**: 8617–25. https://doi.org/10.1093/nar/gkaa551

9 Wilcox B, Osterman I, Serebryakova M *et al. Escherichia coli* ItaT is a type II toxin that inhibits translation by acetylating isoleucyl-tRNA^{Ile}. *Nucleic Acids Res* 2018; **46**: 7873–85. https://doi.org/10.1093/nar/gky560

10 Cheverton AM, Gollan B, Przydacz M *et al.* A *Salmonella* toxin promotes persister formation through acetylation of tRNA. *Mol Cell* 2016; **63**: 86–96. https://doi.org/10.1016/j.molcel.2016.05.002

11 CoRycroft JA, Gollan B, Grabe GJ *et al.* Activity of acetyltransferase toxins involved in *Salmonella* persister formation during macrophage infection. *Nat Commun* 2018; **9**: 1993. https://doi.org/10.1038/s41467-018-04472-6

12 Grabe GJ, Giorgio RT, Hall AMJ *et al.* Auxiliary interfaces support the evolution of specific toxin-antitoxin pairing. *Nat Chem Biol* 2021; **17**: 1296–304. https://doi.org/10.1038/s41589-021-00862-y

13 McVicker G, Tang CM. Deletion of toxin-antitoxin systems in the evolution of *Shigella sonnei* as a host-adapted pathogen. *Nat Microbiol* 2017; **2**: 16204. https://doi.org/10.1038/nmicrobiol.2016.204

14 Liu P, Li P, Jiang X *et al.* Complete genome sequence of *Klebsiella pneumoniae* subsp pneumoniae HS11286, a multidrug-resistant strain isolated from human sputum. *J Bacteriol* 2012; **194**: 1841–2. https://doi.org/10.1128/JB.00043-12

15 Qian H, Yao Q, Tai C *et al.* Identification and characterization of acetyltransferase-type toxin-antitoxin locus in *Klebsiella pneumoniae*. *Mol Microbiol* 2018; **108**: 336–49. https://doi.org/10.1111/mmi.13934

16 LeRoux M, Culviner PH, Liu YJ *et al.* Stress can induce transcription of toxin-antitoxin systems without activating toxin. *Mol Cell* 2020; **79**: 280–92. https://doi.org/10.1016/j.molcel.2020.05.028

17 Muthuramalingam M, White JC, Bourne CR. Toxin-antitoxin modules are pliable switches activated by multiple protease pathways. *Toxins (Basel)* 2016; **8**: 214. https://doi.org/10.3390/toxins8070214

18 Ronneau S, Helaine S. Clarifying the link between toxin-antitoxin modules and bacterial persistence. *J Mol Biol* 2019; **431**: 3462–71. https://doi.org/10.1016/j.jmb.2019.03.019

19 Overgaard M, Borch J, Jorgensen MG *et al.* Messenger RNA interferase RelE controls *relBE* transcription by conditional cooperativity. *Mol Microbiol* 2008; **69**: 841–57. https://doi.org/10.1111/j.1365-2958.2008.06313.x

20 Garcia-Pino A, Balasubramanian S, Wyns L *et al.* Allostery and intrinsic disorder mediate transcription regulation by conditional cooperativity. *Cell* 2010; **142**: 101–11. https://doi.org/10.1016/j.cell.2010.05.039

21 Qian H, Yu H, Li P *et al.* Toxin-antitoxin operon *kacAT* of *Klebsiella pneumoniae* is regulated by conditional cooperativity via a W-shaped KacA-KacT complex. *Nucleic Acids Res* 2019; **47**: 7690–702. https://doi.org/10.1093/nar/gkz563

22 Bordes P, Genevaux P. Control of toxin-antitoxin systems by proteases in *Mycobacterium tuberculosis*. *Front Mol Biosci* 2021; **8**: 691399. https://doi.org/10.3389/fmolb.2021.691399

23 Dubiel A, Wegrzyn K, Kupinski AP *et al.* ClpAP protease is a universal factor that activates the *parDE* toxin-antitoxin system from a broad host range RK2 plasmid. *Sci Rep* 2018; **8**: 15287. https://doi.org/10.1038/s41598-018-33726-y

24 Lunge A, Gupta R, Choudhary E *et al.* The unfoldase ClpC1 of *Mycobacterium tuberculosis* regulates the expression of a distinct subset of proteins having intrinsically disordered termini. *J Biol Chem* 2020; **295**: 9455–73. https://doi.org/10.1074/jbc.RA120.013456

25 Maisonneuve E, Shakespeare LJ, Jorgensen MG *et al.* Bacterial persistence by RNA endonucleases. *Proc Natl Acad Sci U S A* 2011; **108**: 13206–11. https://doi.org/10.1073/pnas.1100186108

26 Pu Y, Zhao Z, Li Y *et al.* Enhanced efflux activity facilitates drug tolerance in dormant bacterial cells. *Mol Cell* 2016; **62**: 284–94. https://doi.org/10.1016/j.molcel.2016.03.035

27 Griffith KL, Wolf RE. Measuring beta-galactosidase activity in bacteria: cell growth, permeabilization, and enzyme assays in 96-well arrays. *Biochem Bioph Res Co* 2002; **290**: 397–402. https://doi.org/10.1006/bbrc.2001.6152

28 Livak KJ, Schmittgen TD. Analysis of relative gene expression data using real-time quantitative PCR and the $2^{-\Delta\Delta C_T}$ method. *Methods* 2001; **25**: 402–8. https://doi.org/10.1006/meth.2001.1262

29 Haddadin FT, Kurtz H, Harcum SW. Serine hydroxamate and the transcriptome of high cell density recombinant *Escherichia coli* MG1655. *Appl Biochem Biotechnol* 2009; **157**: 124–39. https://doi.org/10.1007/s12010-008-8241-0

30 Zhou X, Eckart MR, Shapiro L. A bacterial toxin perturbs intracellular amino acid balance to induce persistence. *mBio* 2021; **12**: e03020-20. https://doi.org/10.1128/mBio.03020-20

1 **Antibiotic-induced degradation of antitoxin enhances the transcription of**

2 **acetyltransferase-type toxin-antitoxin operon**

3

4 **Supplementary data**

5

6 **Supplemental methods**

7 **Table S1.** Strains and plasmids used in this study.

8 **Table S2.** Oligonucleotides used in this study.

9 **Figure S1.** Different *K. pneumoniae* strains were treated with meropenem or imipenem.

10 **Figure S2.** The influence of fluorescent protein on the function of KacA and KacT.

11 **Figure S3.** Meropenem induces KacA-eGFP degradation through Lon protease.

12 **Figure S4.** Imipenem induces KacA-eGFP degradation through Lon protease.

13 **Figure S5.** KacT was not degraded under the condition of meropenem.

14 **Figure S6.** Meropenem reduces the ratio of KacA: KacT.

15 **Figure S7.** Transcription analysis of *kacAT* promoter by *lacZ* fusions.

16

Supplemental methods

Bacterial strains, plasmids and conditions

Details of all the strains, plasmids and primers used in this study are listed in

Supplementary Table S1 and Table S2. The pBAD33-carrying *K. pneumoniae* was

cultivated in Luria-Bertani (LB) broth medium at 37℃, supplemented with

chloramphenicol (30 μg/mL). Due to pBAD33 containing an arabinose-induced

promotor, *araBAD*, 0.2% (w/v) of arabinose added to the culture was used to induce

araBAD expression, while glucose (0.2%, w/v) was used to inhibit.

Plasmid construction

To construct plasmids for tolerance assay and western-blot, the single *kacT* gene

(*KPHS_05890*) and the entire *kacAT* operon (*KPHS_05880-KPHS_05890*) were cloned

into pBAD33 plasmid, respectively. Briefly, the *kacT* gene and *kacAT* operon, including

their native ribosome binding sites, were amplified from the genomic DNA of *K.

pneumoniae* HS11286 and the corresponding primers used are shown in Table S2. The

PCR products were digested with enzyme (*Sac*I-*Hind*III) and then cloned into pBAD33

using T4 DNA ligase, resulting in the plasmids pBAD33-*kacT,* pBAD33-*kacAT*, pBAD33-

6×His-kacA, pBAD33-*6×His-kacAT*, and pBAD33-*Myc-kacT*, respectively. The plasmids

were transformed into HS11286-RR2 or HS11286-RR2*ΔkacAT*.

Point mutation

To construct the point mutation plasmids for pBAD33-kacA^{R8A} (at the eighth amino

residue of KacA) and pBAD33-Myc-kacT^{Y145F} (at the 145th amino residue of KacT),

pBAD33-kacA and pBAD33-Myc-kacT were first constructed. Then, the

QuickMutation™ Site-Directed Mutagenesis Kit (Category No.: D0206), provided by

40 Beyotime Biotechnology (Shanghai, China), was used to construct the point mutation

41 plasmids. We performed the point mutation assay following the manufacturer's

42 instructions in the kit.

43 ***Strains construction***

44 The *K. pneumoniae* HS11286-RR2Δ*lon* and HS11286-RR2Δ*kacAT* strains were

45 constructed by λ-Red to replace the *lon* or *kacAT* genes with hygromycin resistance

46 (*hph*) cassette with homology flanking the *lon* or *kacAT* regions. The hygromycin

47 resistance cassette was removed by pFLP2 excision. The antibiotic resistance

48 cassettes were amplified using SOE-PCR (Gene splicing by overlap extension PCR).

49 The DNA-binding mutant (*kacA*[R8A]) was constructed by allelic exchange (**Figure 2A**),

50 wherein the kacAT locus was first replaced with the *hph-sacB* cassette. Then the DNA-

51 binding mutant allele was amplified from pBAD33-kacA[R8A] with a flanking homology

52 region through SOE-PCR. Furthermore, the *hph-sacB* cassette was finally replaced by

53 the *kacA*[R8A] cassette. The tool plasmid used for λ-Red recombination is pKOBEG.[1] All

54 the primers used for strain construction are listed in Table S2.

55 ***Fluorescent Microscopy***

56 All the fluorescence pictures were taken on an inverted microscope (Leica TCS

57 SP8 STED). Firstly, the *kacA* and *kacT* genes (fused with eGFP and mCherry,

58 respectively) were cloned into the pCDFDuet plasmid. Then the pCDFDuet plasmid

59 expressing *kacA-eGFP* and *mCherry-kacT* was transformed into *E. coli* BL21(DE3).

60 Overnight cultured strains were re-inoculated into fresh LB broth medium (1:100) to an

61 OD_{600} = 0.5. 10 μL of the bacterial culture was transferred to an LB agar block

62 supplemented with 0.5 mM IPTG and placed into the microscope chamber of a Leica

63   inverted microscope.[2] The illumination was provided by different lasers, at 488 nm for

64   eGFP and 587 nm for mCherry.

65   ***Microplate reader***

66   pBAD33 plasmids that express *kacA* or *kacT* fused to fluorescent protein were

67   transformed into wild-type RR2 or *lon*-deletion (RR2*Δlon*) cells. The transformants were

68   grown in the LB medium at 37℃, when OD_{600} = 0.3, 0.2 % (w/v) of arabinose was

69   added. After 90 minutes of induction, 0.2 % (w/v) of glucose was added to inhibit

70   pBAD33 expression together with meropenem. The fluorescence values of samples

71   collected at the indicated time points were read by a microplate reader (SpectraMax

72   iD5, Molecular Devices, USA).

73   ***A quantitative model of kacAT expression dynamics***

74   We consider transcript m expression from a promoter with transcription activity φ,

75   which is degraded with rate λ_m:

76    $$\frac{\mathrm{d}m}{\mathrm{d}t} = \varphi - \lambda_m m. \tag{1.1}$$

77   By using the common assumption that transcripts are in quasi-equilibrium, i.e.,

78    $\mathrm{d}m/\mathrm{d}t = 0$, we obtain:

79    $$m = \frac{\varphi}{\lambda_m}. \tag{1.2}$$

80   In overexpression experiments, when transcripts are expressed from a constitutive

81   promoter with transcript activity φ_0, the above expression leads to:

82    $$m = \frac{\varphi_0}{\lambda_m}. \tag{1.3}$$

83   In the native (wild-type) system, the promoter is regulated (repressed) by *4A2T* (*A*

84 standing for antitoxin and *T* for the toxin) so that the transcription activity corresponds

85 to:

86
$$\varphi = \frac{\varphi_0}{1 + \dfrac{[4A2T]}{K_D}},$$
(1.4)

87 Where φ_0 is the basal promoter transcription rate, $[4A2T]$ is the complex

88 concentration, and K_D is the dissociation constant of the complex binding to the

89 promoter.

90 The protein (antitoxin and toxin) dynamics is determined by:

91
$$\frac{dA}{dt} = K_A m - (\lambda_C + \Delta\lambda)A - 4\lambda_C[4A2T]$$
(1.5)

92
$$\frac{dT}{dt} = K_T m - \lambda_C T - 2\lambda_C[4A2T],$$
(1.6)

93 Where K_A and K_T are, respectively, the antitoxin and toxin translation rates, λ_C is the

94 protein dilution rate, and $\Delta\lambda$ is the rate of the active antitoxin degradation (through e.g.,

95 Lon activation).

96 The terms on the right-hand-sides of Eqs. (1.5) and (1.6) are (in the order from left

97 to right): protein translation from the transcript, protein clearance by either dilution or

98 active degradation (for A under stress conditions), and complex clearance (here

99 assumed also by dilution). Complex clearance leads to the loss of 4 *A* units and 2*T*

100 units, leading to the prefactors 4 and 2 in the last terms on the right-hand-sides of the

101 differential equations.

102 In the differential equations above, we assume that the formation of $4A2T$

103 complex is in quasi-equilibrium, i.e., that for the reactions:

104
$$4A + 2T \underset{K_-}{\overset{K_+}{\rightleftharpoons}} [4A2T] \overset{\lambda_c}{\longrightarrow} 0, \tag{1.7}$$

105    $d[4A2T]/dt = 0$, so that:

106
$$K_+ A^4 T^2 - K_-[4A2T] - \lambda_c[4A2T] = 0. \tag{1.8}$$

107   By further assuming that the complex kinetics is much faster than the protein

108   dilution ($K_- \gg \lambda_c$), we obtain:

109
$$[4\,A\,2\,T] = \frac{K_+}{K_-} A^4 T^2 = \frac{A^4 T^2}{K^5}, \tag{1.9}$$

110   Where $K^5 \equiv K_- / K_+$ is the complex dissociation constant (K having the dimension of

111   concentration).

112   To obtain a steady state (equilibrium) for the system, we equate dA/dt and

113   dT/dt with zero. Given that A's translation rate is larger than T's, we further assume

114    $K_A = 2K_T$, reflecting the stoichiometric ratio of A and T in $4A2T$ complex, and

115   allowing to considerably simplify further mathematical relations.

116   From Eqs. (1.5) and (1.6) we further obtain (A^* and T^* indicate the equilibrium

117   values):

118
$$A^* = \frac{2\lambda_C}{\lambda_C + \Delta\lambda} T^*. \tag{1.10}$$

119   Note that by using the relation above, we can simplify finding A^* and T^* from Eqs.

120   (1.5) and (1.6), by finding roots of only one non-linear equation – rather than by solving

121   the system of two non-linear differential equations. To reduce the number of parameters

122   and make the quantities dimensionless, we rescale the equations in the way described

123   below.

124   ***Numerically solving the model***

125   To reduce the number of parameters and make the quantities dimensionless, we

126   rescale the equations in the following way: $\tilde{m} = m/K$, $\tilde{A} = A/K$, and $\tilde{T} = T/K$,

127   corresponding to rescaled concentrations of *kacAT* transcript, KacA and KacT; time is

128   made dimensionless by $\tau = \lambda_c t$, while the other two rates are made dimensionless by

129   rescaling with λ_C, $\tilde{K}_T = K_T/\lambda_C$ and $\Delta\tilde{\lambda} = \Delta\lambda/\lambda_C$. Finally, $\tilde{K}_B = K/K_D$ is the rescaled

130   binding affinity of $4A2T$ to the promoter *DNA* and $\tilde{\varphi} = \varphi_0/(\lambda_m K)$ is the rescaled

131   (dimensionless) expression rate.

132   With such rescaling, the differential equations for KacA and KacT expressions become:

$$\frac{d\tilde{A}}{d\tau} = 2\tilde{K}_T\tilde{m} - (1+\Delta\tilde{\lambda})\tilde{A} - 4\tilde{A}^4\tilde{T}^2 \qquad \textbf{(1.11)}$$

133

$$\frac{d\tilde{T}}{d\tau} = \tilde{K}_T\tilde{m} - \tilde{T} - 2A^4T^2. \qquad \textbf{(1.12)}$$

134

135   XPPAUT[3] is used to simulate the dynamics of the system above, with the preferences

136   nmash=100, dt=0.005, total=50, bounds=1e3, maxtor=1 000 000. XPPAUT was also

137   used to calculate and display KacA and KacT nullclines, whose intersection determines

138   the system's steady state. Trajectories were shown in the phase plane by simulating the

139   system dynamics for different initial conditions. The stability of the steady state was

140   analyzed through 'sing pts' (singular points) option in XPPAUT. The phase plane

141   analysis was visualized in XPPAUT.

142   To investigate how the equilibrium values of KacA, KacT proteins and *kacAT*

143   transcripts depend on $\tilde{K}_B$ (binding strength of $4A2T$ complex to the promoter) and $\Delta\tilde{\lambda}$

144   (the rate of KacA active degradation), we numerically solve the following equation for

145    $\tilde{T}^*$ (see Eqs. (1.1), (1.12) at equilibrium and corresponding rescaled quantities, plus

7

146 Eqs. (1.4), (1.10); here * indicates equilibrium value):

$$0 = \tilde{K}_T \frac{\tilde{\varphi}}{1 + \tilde{K}_B \left(\frac{2}{1 + \Delta\tilde{\lambda}} \right)^4 \tilde{T}^{*6}} - \tilde{T}^* - 2\left(\frac{2}{1 + \Delta\tilde{\lambda}} \right)^4 \tilde{T}^{*6}. \qquad \textbf{(1.13)}$$

148 Roots (zeros) of this equation are found by using the MATLAB 'fsolve' function. Once

149 $\tilde{T}^*$ is found, $\tilde{A}^*$ and $\tilde{m}^*$ are found by:

$$\tilde{A}^* = \frac{2}{1 + \Delta\tilde{\lambda}} \tilde{T}^*, \qquad \textbf{(1.14)}$$

151 and

$$\tilde{m}^* = \frac{\tilde{\varphi}}{1 + \tilde{K}_B \left(\frac{2}{1 + \Delta\tilde{\lambda}} \right)^4 \tilde{T}^{*6}}, \qquad \textbf{(1.15)}$$

153 as derived in the previous subsection. Note that the solutions above for $\tilde{K}_B = 0$

154 correspond to the constitutive (unregulated) case. The dependence of the equilibrium

155 for values for $\tilde{A}^*$, $\tilde{T}^*$ and $\tilde{m}^*$ on $\tilde{K}_B$ and $\Delta\tilde{\lambda}$ was visualized in MATLAB.

156 **Statistical analysis**

157 　　All the results were expressed as means ± SD. Furthermore the statistical

158 significance of differences between different groups was analyzed by unpaired

159 Student's *t*-test using the R program (https://www.r-project.org/). $P < 0.05$ was

160 considered to be statistically significant.

161
162

163 **Table S1.** Strains and plasmids used in this study

Strain/plasmid	Description	Source or Reference
Strain		
K. pneumoniae:		
HS11286-RR2	Δ*bla*KPC-2Δ*KPHS_p300510-KPHS_p300880* (Δ*bla*KPC-2ΔMDR)	4
HS11286-RR2Δ*lon*	HS11286-RR2 *lon* in frame deletion derivative	This study
HS11286-RR2Δ*kacAT*	HS11286-RR2 *kacAT* in frame deletion derivative	This study
HS11286-RR2Δ(*kacAT lacZ*)	HS11286-RR2 *kacAT* and *lacZ* in frame deletion derivative	This study
HS11286-RR2Δ(*lon kacAT lacZ*)	HS11286-RR2 *kacAT, lon and lacZ* in frame deletion derivative	This study
E. coli:		
E. coli BL21 (DE3)	F–, *ompT*, *gal*, *dcm*, *lon*, *hsdSB*, (rB- mB-) λ(DE3)	Novagen
Plasmid		
pBAD33	p15A ori; araC; P*ara* promoter, Cml^R	5
pBAD33+*kacT*	pBAD33 bearing *kacT* and its SD sequence as an *Sac*I-*Hind*III insert	This study
pBAD33+*kacAT*	pBAD33 bearing *kacAT* and its SD sequence as an *Sac*I-*Hind*III insert	This study
pBAD33+6×His-*kacA*	pBAD33 bearing 6×His labeled *kacA* and its SD sequence as an *Sac*I-*Hind*III insert	This study
pBAD33+6×His-*kacA-kacT*	pBAD33 bearing 6×His labeled *kacA* with *kacT* and its SD sequence as an *Sac*I-*Hind*III insert	This study
pBAD33+Myc-*kacT*^Y145F	pBAD33 bearing Myc labeled *kacT*^Y145F and its SD sequence as an *Sac*I-*Hind*III insert	This study
pBAD33+*kacT-mCherry*	pBAD33 bearing *kacT-mCherry* as an *Sac*I-*Hind*III insert	This study
pBAD33+*mCherry-kacT*	pBAD33 bearing *mCherry-kacT* as an *Sac*I-*Hind*III insert	This study
pBAD33+*kacT*+*eGFP-kacA*	pBAD33 bearing *kacT* with *eGFP-kacA* as an *Sac*I-*Hind*III insert	This study
pBAD33+*kacT*+*kacA-eGFP*	pBAD33 bearing *kacT* with *kacA-eGFP* as an *Sac*I-*Hind*III insert	This study
pBAD33+*mCherry-kacT*+*kacA*	pBAD33 bearing *mCherry-kacT* with *kacA* as an *Sac*I-*Hind*III insert	This study
pBAD33+*mCherry-kacT*+*eGFP-kacA*	pBAD33 bearing *mCherry-kacT* with *eGFP-kacA* as an *Sac*I-*Hind*III insert	This study
pBAD33+*mCherry-kacT*+*kacA-eGFP*	pBAD33 bearing *mCherry-kacT* with *kacA-eGFP* as an *Sac*I-*Hind*III insert	This study
pBAD33+*kacA-eGFP*	pBAD33 bearing *kacA-eGFP* as an *Sac*I-*Hind*III insert	This study
pBAD33+*kacA-eGFP-kacT*	pBAD33 bearing *kacA-eGFP* with *kacT* as an *Sac*I-*Hind*III insert	This study
pCD (pCDFDuet)	T7 promoter, KanaR	Novagen
pCD+*mCherry-kacT*+*kacA-eGFP*	pCD bearing *mCherry-kacT* with *kacA-eGFP* as an *Sac*I-*Hind*III insert	This study
pLacZ-P*kacAT*	pLACZ derivative with promoter of *kacAT* operon inserted upstream of *lacZ*	This study

164

165 **Table S2.** Oligonucleotides used in this study.

Name	Sequence (5'-3')
KacTF	CGAGCTCAGGTAAGGTAGAGCTAATGGAGC
KacTR	CAAGCTTTTAGCTGCTGCCTGACTCATCGTCAGTAAAGAGCT
KacATF	GAGCTCAACAGGCCGGAGATAACGTA
KacATR	CAAGCTTTTAGCTGCTGCCTGACTCATCGTCAGTAAAGAGCT
6×His-kacAF	GAGCTCATGCATCACCATCATCACCACATGCCCGCACTTAAAAAGC
6×His-kacAR	CCAAGCTTTTACCTGGTTTGTAGACGCTTCGCTGCACG
6×His-kacATF	GAGCTCATGCATCACCATCATCACCACATGCCCGCACTTAAAAAGC
6×His-kacATR	CAAGCTTTTAGCTGCTGCCTGACTCATCGTCAGTAAAGAGCT
Myc-kacT^{Y145F}F	ATCACCATCATCACCACTAAGGTAGAGCTAATGGAGCAGC
Myc-kacT^{Y145F}R	TCTCATCCGCCAAAACAGCCAAGCTTTTACAGATCCTCTTCTGAGATGAG
RTkacTF	TAAGGGGTTATGCGCTGGTC
RTkacTR	TTACGCTTGGCGCATTTTGA
RTkacAF	AGAGCATCATCGAGGAAGCTGC
RTkacAR	CCTCCATCACCAGGCTCCATGAT
RTgapAF	GCGCTAACTTCGACGCTTAC
RTgapAR	GGTCATCAGGCCTTCAACGA
KacAEF	CGAGCTCATGCCCGCACTTAAAAAGCAG
KacAER	TGCTCCATTAGCTCTACCTTACTTGTACAGCTCGTCCAT
KacTEF	CAAGTAAGGTAGAGCTAATGGAGCAGCAACTGACGAT
KacTER	CCAAGCTTTTATGACTCATCGTCAGTAAAG
mkacTF	GAGCTCATGGTGAGCAAGGGTGAGGA
mkacTR	AAGCTTTTATGACTCATCGTCAGTAAAG
KacTmF	CGAGCTCATGGAGCAGCAACTGACGAT
KacTmR	CCAAGCTTCTACTTGTACAGCTCGTCCATG
ekacAF	CGAGCTCATGGCCACAACCATGGTGAG
ekacAR	CCAAGCTTTTACCTGGTTTGTAGACGCT
NkacAEF	GACGAGCTGTACAAGATGCCCGCACTTAAAAAGCAG
NkacAER	TTTAAGTGCGGGCATCTTGTACAGCTCGTCCATGC
CkacAEF	CGTCTACAAACCAGGATGGTGAGCAAGGGCGAGGAG
CkacAER	GCCCTTGCTCACCATCCTGGTTTGTAGACGCTTCG
NkacTMF	GACGAGCTGTACAAGATGGAGCAGCAACTGACGAT
NkacTMR	CAGTTGCTGCTCCATCTTGTACAGCTCGTCCATGC
CkacTMF	CTGACGATGAGTCAATGGTGAGCAAGGGTGAGGAG
CkacTMR	CCCTTGCTCACCATTGACTCATCGTCAGTAAAGAG
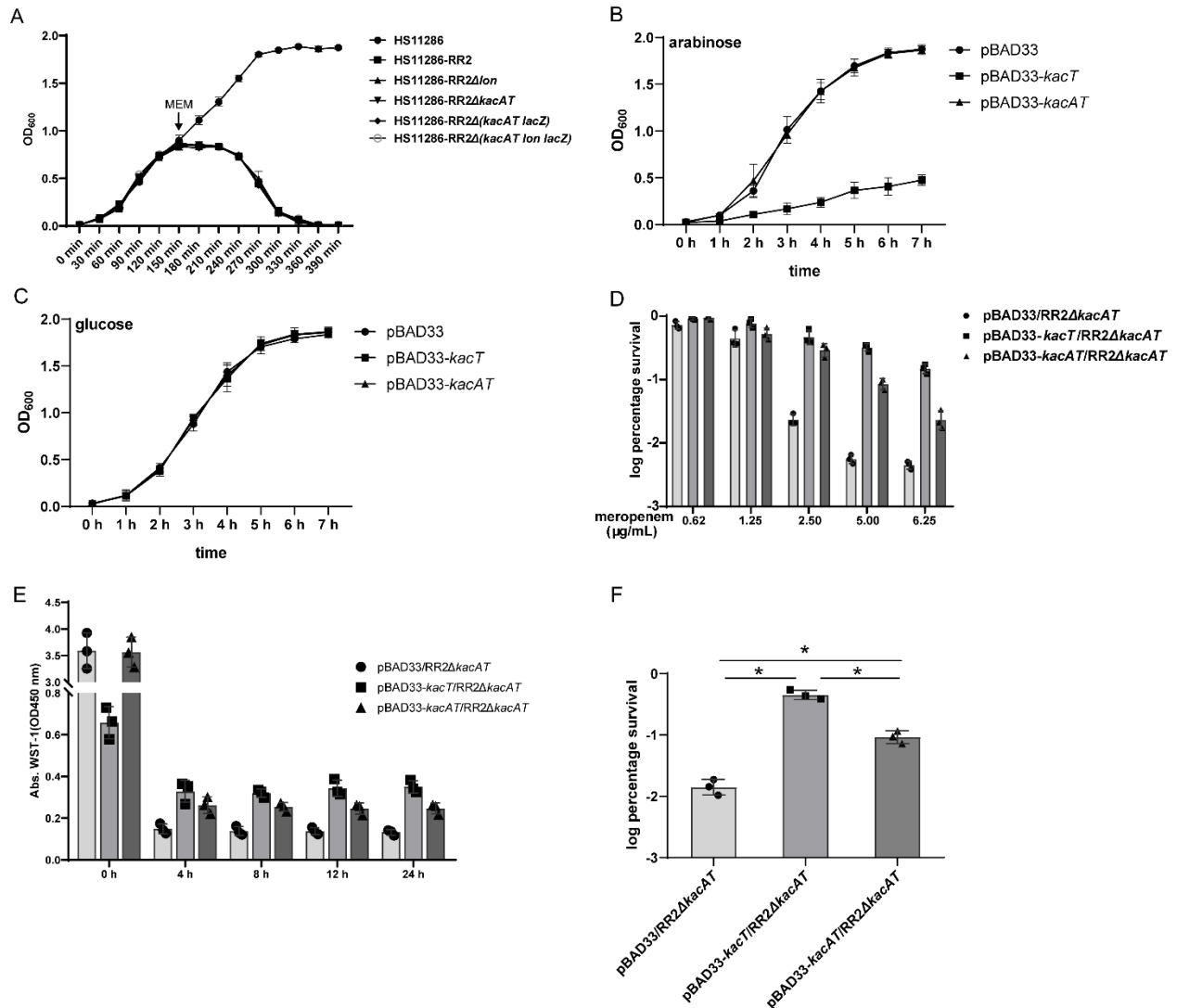
166

167

Figure S1. Different *K. pneumoniae* strains were treated with meropenem or imipenem.

(**A**) Growth curves of different *K. pneumoniae* strains. The overnight culture was

inoculated into fresh LB at 1:100, and then 5 µg/mL of meropenem was added at 150

minutes (logarithmic phase). The OD_{600} of each culture was measured every 30 minutes

until 390 minutes. (**B-C**) Growth curves of *K. pneumoniae* HS11286-RR2Δ*kacAT* strain

expressing KacT, KacAT or empty pBAD33 plasmid. (**D**) The *kacAT* knockout strain

RR2Δ*kacAT* that harbors the empty vector pBAD33, KacT-expressing vector (pBAD33-

175   *kacT*), or KacAT-expressing vector (pBAD33-*kacAT*) was exposed to a differential

176   concentration of meropenem for four hours. (**E**) Enzymatic activity by colorimetric assay

177   (WST-1-based) of *K. pneumoniae* HS11286-RR2Δ*kacAT* expressing KacT, KacAT or

178   empty pBAD33 plasmid in the presence of meropenem. The enzymatic activity was

179   measured by using WST-1 protocol (Beyotime Biotechnology, Shanghai, China) (**F**) The

180   survival of RR2Δ*kacAT* harboring pBAD33-*kacT,* pBAD33-*kacAT,* or pBAD33 after

181   treating with 5 μg/mL of imipenem for four hours. The survival percentage was

182   calculated by dividing the cfu/mL of the antibiotic-treated culture by the cfu/mL of the

183   culture before adding antibiotic. The bar represents the mean of three independent

184   experiments, and the error bar indicates the SD (* p-value < 0.05).
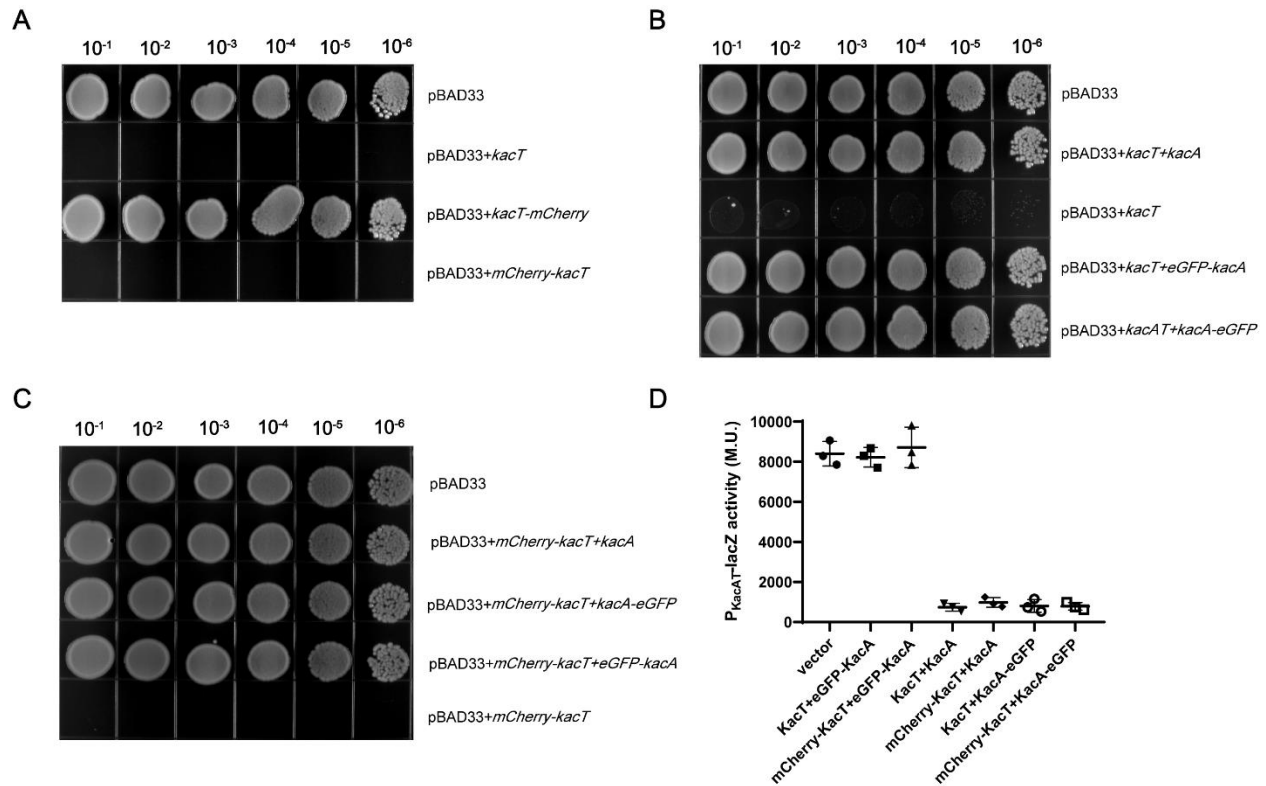
Figure S2. The influence of fluorescent protein on the function of KacA and KacT. (**A-C**) Growth of *K. pneumoniae* HS11286-RR2Δ*kacAT* containing the different plasmids. The strain was serially diluted and plated on LB agar supplemented with 30 μg/mL chloramphenicol and 0.2 % arabinose (w/v). (**D**) LacZ activity of *K. pneumoniae* HS11286-RR2Δ*(kacAT lacZ)* harboring P_{kacAT} promoter-*lacZ* fusions in the presence of various combinations of KacA and KacT. LacZ activity was measured 5 h after the addition of IPTG (0.5 mM) to induce *kacA* and *kacT*.
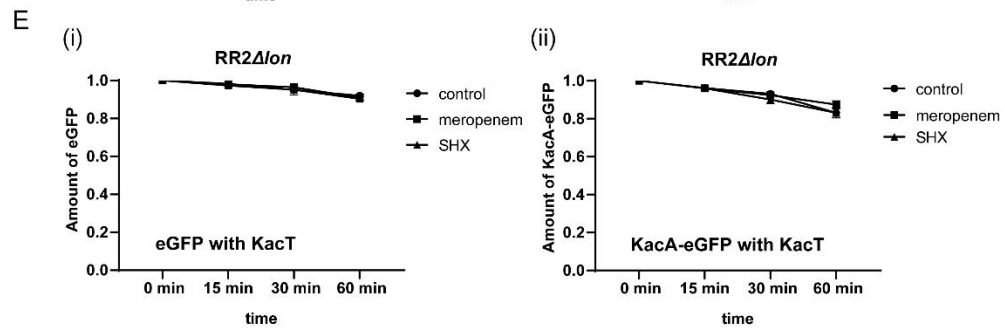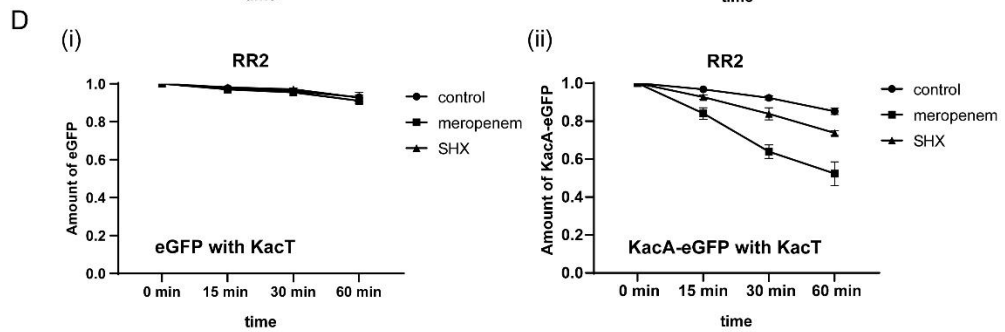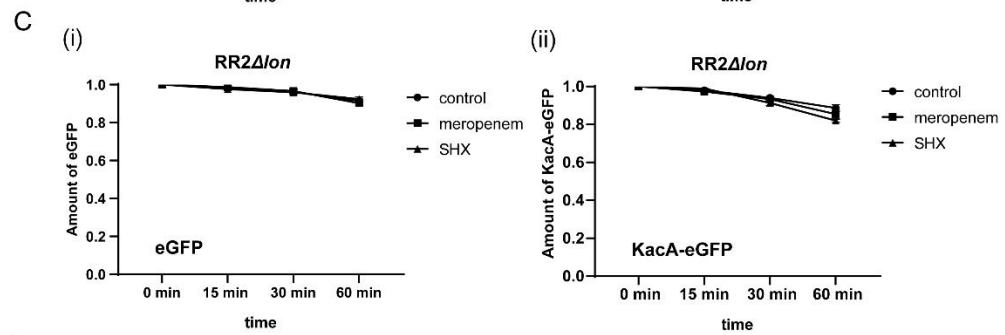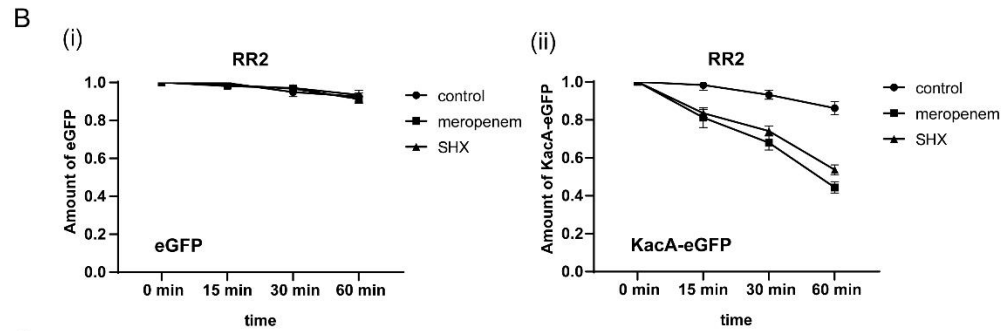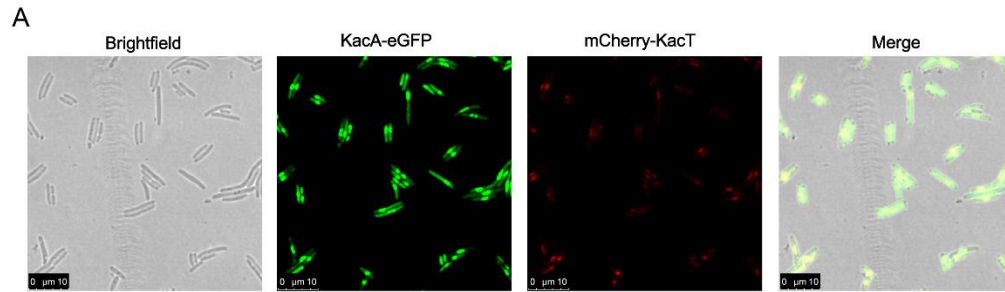
Figure S3. Meropenem induces KacA-eGFP degradation through Lon protease. (A)

197 Fluorescence microscope showed the expression of KacA-eGFP and mCherry-KacT in

198 *E. coli* BL21 (DE3). After transforming the pCDFDuet plasmid expressing KacA-eGFP

199 and mCherry-KacT into *E. coli* BL21 (DE3), the strain was incubated on LB agar

200 supplemented with 0.5 mM IPTG, and the expression of KacA and KacT was

201 photographed using fluorescence microscopy. Wild-type RR2 and *lon*-deletion

202 (RR2*Δlon*) strains harboring the pBAD33 vector that expresses **(B-C)** only KacA-eGFP

203 or eGFP and **(D-E)** with KacT. The strains were grown in LB medium at 37℃, when

204 $OD_{600} = 0.3$, 0.2 % (w/v) of arabinose was added. After 90 minutes of induction, 0.2 %

205 (w/v) of glucose was added to inhibit KacA-eGFP expression together with meropenem.

206 The fluorescence intensity of samples collected at the indicated time points was

207 measured by a microplate reader. SHX was used to compare with meropenem. Data

208 were presented as mean ± SD; $n = 3$.

209

210
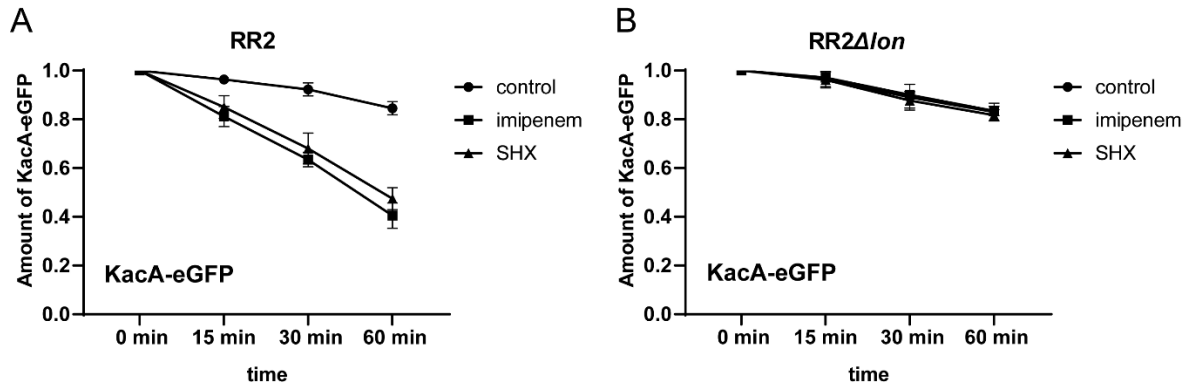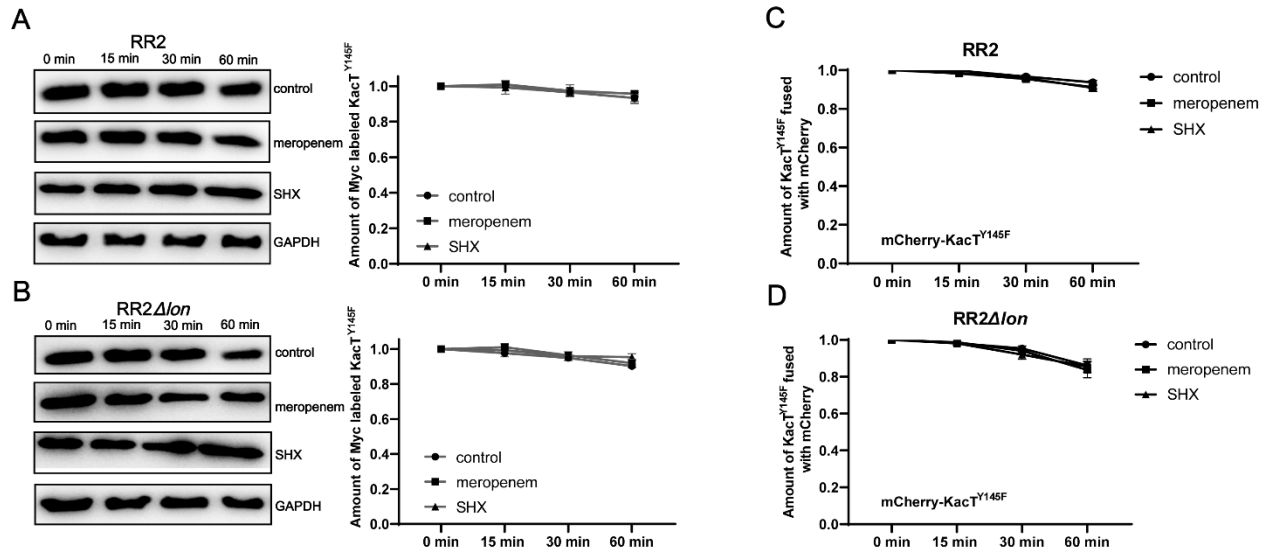
Figure S4. Imipenem induces KacA-eGFP degradation through Lon protease. Wild-type

RR2 (**A**) or RR2*Δlon* (**B**) containing the pBAD33 vector that expresses KacA-eGFP. The

fluorescence intensity of *K. pneumoniae* cells after treatment with imipenem was

measured in the same method as Figure S3. SHX was used to compare with imipenem.

Data were presented as mean ± SD; *n* = 3.

219

Figure S5. KacT was not degraded under the condition of exposure to meropenem. The

wild-type strain RR2 and the Lon protease gene deletion strain RR2Δ*lon* harboring

KacT^{Y145F} **(A-B)** or mCherry-KacT^{Y145F} **(C-D)** on pBAD33 vector were grown in LB

medium at 37℃, at OD$_{600}$ = 0.3, 0.2 % (w/v) of arabinose was added. After 90 min

induction, 0.2 % (w/v) of glucose was added to inhibit the expression of KacT. Then,

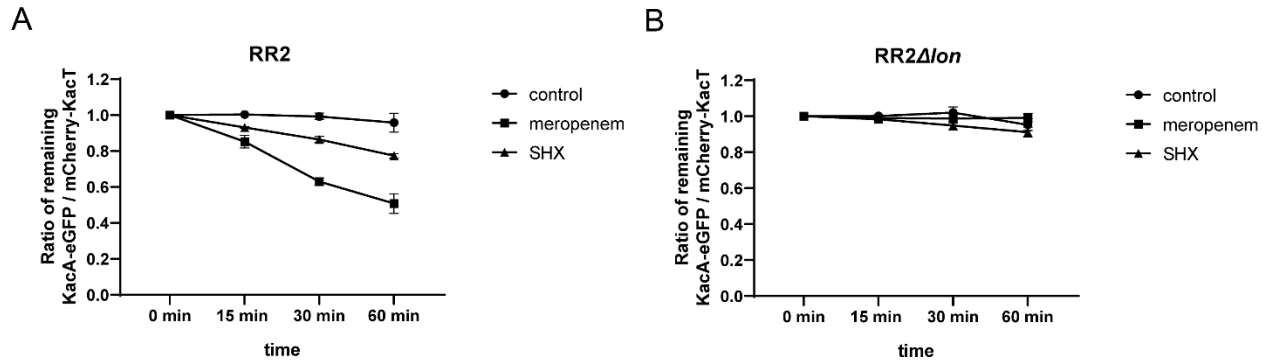meropenem (MEM) was added to the culture medium, and samples for western-blot and

fluorescence intensity were collected at the indicated time (0-, 15-, 30- and 60-minutes).

The fluorescence intensity were measured by a microplate reader. SHX was used to

compare with meropenem. Data were presented as mean ± SD; *n* = 3.

229

230

17

Figure S6. Meropenem reduces the ratio of KacA: KacT. The ratio of remaining KacA-eGFP to mCherry-KacT in RR2 **(A)** or RR2Δ*lon* **(B)** under the treatment of meropenem. pBAD33 vector that expresses both KacA-eGFP and mCherry-KacT was transformed into RR2 or RR2Δ*lon*. The strains were grown in LB broth at 37℃, 0.2 % (w/v) of arabinose was added in the medium when OD_{600} = 0.3. After 90 minutes of induction, 0.2 % (w/v) of glucose and 5 µg/mL meropenem were added. The fluorescence values of samples collected at the indicated time points were measured by a microplate reader. SHX was used to compare with meropenem. Data were presented as mean ± SD; *n* = 3.
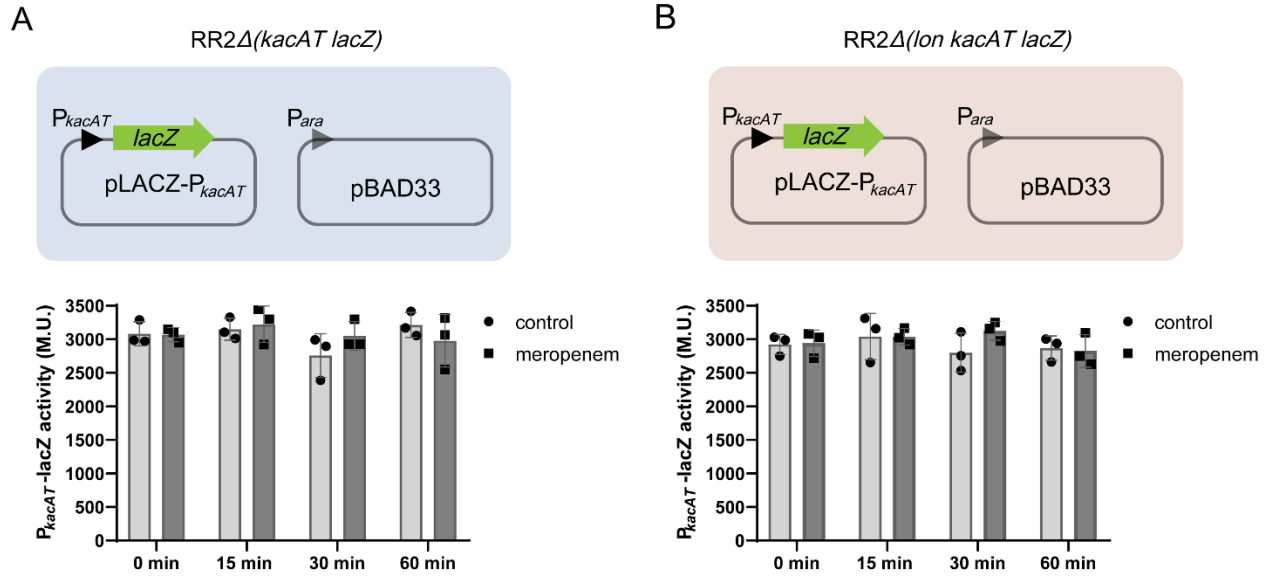
Figure S7. Transcription analysis of *kacAT* promoter by *lacZ* fusions. *kacAT* promoter

(P*kacAT*) and the downstream *lacZ* were cloned on the pLACZ-P*kacAT* plasmid. The

combinations of pLACZ-P*kacAT* and empty pBAD33 were co-transformed into the

RR2Δ*(kacAT lacZ)* cells **(A)** and the RR2Δ*(lon kacAT lacZ)* cells **(B)**. Meropenem and

0.2% of glucose were added after 3 h of induction of KacA and KacT by arabinose

(0.2%). Samples for enzymatic activities were collected at the indicated time points (0-,

15-, 30-, and 60-minutes).

References

1   Chaveroche MK, Ghigo JM, d'Enfert C. A rapid method for efficient gene replacement in the filamentous fungus *Aspergillus nidulans*. *Nucleic Acids Res* 2000; **28**: E97.

2   Wilcox B, Osterman I, Serebryakova M *et al*. *Escherichia coli* ItaT is a type II toxin that inhibits translation by acetylating isoleucyl-tRNA^{Ile}. *Nucleic Acids Res* 2018; **46**: 7873-85.

3   Ermentrout, B , Mahajan, A Simulating, analyzing, and animating dynamical systems: a Guide to XPPAUT for researchers and students. *Appl Mech Rev* 2003; **56**: B53.

4   Bi D, Jiang X, Sheng Z-K *et al*. Mapping the resistance-associated mobilome of a carbapenem-resistant *Klebsiella pneumoniae* strain reveals insights into factors shaping these regions and facilitates generation of a 'resistance-disarmed' model organism. *J Antimicrob Chemother* 2015; **70**: 2770-4.

5   Guzman LM, Belin D, Carson MJ *et al*. Tight regulation, modulation, and high-level expression by vectors containing the arabinose P$_{BAD}$ promoter. *J Bacteriol* 1995; **177**: 4121-30.